2011

Estimating Target Vessel Location on Robot-Assisted CABG using Feature-based CT to US Registration

Sungjoon Daniel Cho

Estimating Target Vessel Location on Robot-Assisted CABG using Feature-based CT to US Registration

(Spine title: Estimating target vessel location on robotic assisted CABG)
(Thesis format: monograph)

by

Sungjoon (Daniel) Cho

Graduate Program in Biomedical Engineering

Submitted in partial fulfillment
of the requirements for the degree of
Master of Engineering Science

School of Graduate and Postdoctoral Studies
The University of Western Ontario
London, Ontario, Canada

September 8th, 2011

THE UNIVERSITY OF WESTERN ONTARIO
SCHOOL OF GRADUATE AND POSTDOCTORAL STUDIES

CERTIFICATE OF EXAMINATION

Chief Supervisor

Terry Peters

Co-supervisor

John Barron

Advisory Committee

Dr. Rajni Patel

Dr. Bob Kiaii

Examining Board

Dr. James Lacefield

Dr. David Holdsworth

Dr. David McCarty

The thesis by

Sungjoon (Daniel) Cho

entitled

Estimating Target Vessel Location on Robot-Assisted CABG using Feature-based CT to US Registration

is accepted in partial fulfillment of the
requirements for the degree of
Master of Engineering Science

Chair of Examination Board

Dated this 30th day of August, 2011.

Abstract

Although robot-assisted coronary artery bypass grafting (RA-CABG) has gained more acceptance worldwide, its success still depends on the surgeon's experience and expertise, and the conversion rate to full sternotomy is in the order of $15\% - 25\%$. One of the reasons for conversion is poor pre-operative planning, which is based solely on pre-operative computed tomography (CT) images. This thesis proposes a technique to estimate the global peri-operative displacement of the heart and to predict the intra-operative target vessel location. The technique has been validated via both an *in vitro* and a clinical study, and predicted the position of the peri-operative target vessel location with $\sim$ 3.5 mm RMS accuracy in the *in vitro* study while it yielded $\sim$ 5.0 mm accuracy for the clinical validation. As the desired clinical accuracy imposed by this procedure is on the order of one intercostal space (10 - 15 mm), our technique suits the clinical requirements. It is therefore believed that this technique has the potential to improve the pre-operative planning by updating peri-operative migration patterns of the heart and, consequently, will lead to reduced conversion to conventional open thoracic procedures.

Key words: Image-guided cardiac surgery, Minimally invasive surgery, CABG, rigid-body registration, ultrasound, phantom study

Co-Authorship

The following thesis contains material from manuscripts accepted or submitted for publication.

Part of chapter 3 has been accepted for publication in International Conference on Medical Image Computing and Computer Assisted Intervention as "Predicting Target Vessel Location for Improved Planning of Robot-Assisted CABG Procedure" by Cho, DS., Linte, CA., Chen, E., Wedlake, C., Moore, J., Barron, J., Patel, R., Peters, TM. DS Cho and CA Linte contributed to the experimental design, data acquisition and analysis, and wrote the manuscript. J Moore, C Wedlake and E Chen provided assistance with tool design and also provided suggestions with experimental design and data acquisition. All authors provided editorial assistance and approved the final versions of the manuscripts. The research was performed under the supervision of TM Peters.

Part of chapter 3 and 4 has been submitted for publication in Medical Physcis as "Predicting Target Vessel Location on Robot-Assisted CABG using Feature-based CT to US Registration" by Cho, SD., Linte, CA., Chen, E., Bainbridge, D., Wedlake, C., Moore, J., Barron, J., Patel, R., Peters, TM. DS Cho and CA Linte contributed to the experimental design, data acquisition and analysis, and wrote the manuscript. J Moore, C Wedlake and E Chen provided assistance with tool design and also provided suggestions with experimental design and data acquisition. All authors provided editorial assistance and approved the final versions of the manuscripts. The research was performed under the supervision of TM Peters.

Acknowledgments

I would like to thank Dr. Terry Peters for his support and guidance over the past three years. I would also like to thank Dr. John Barron for his assistance with this work.

Thank you to all of my collegues in the lab, especially Cristian, John, Chris, and Elvis, also the clinicians, Dr. Bob Kiaii, Dr. Daniel Bainbridge, Dr. Gerard Guiraudon and Dr. Doug Jones for helping us with our research. Without their assistance this work would not have been possible.

And, of course, thank you to my friends and family.

Contents

List of Tables

List of Figures

List of Acronyms & Abbreviations

2D	Two-dimensional
3D	Three-dimensional
ACC	American College of Cardiology
ACS	Acute coronary syndrom
AHA	American Heart Association
ARTS	Arterial revascularization therapies study
AVA	Aortic valve annulus
CABG	Coronary artery bypass grafting
CAD	Coronary artery disease
CCAIT	Canadian coronary atherosclerosis intervention trial
CPB	Cardio pulmonary bypass
CT	Computed tomography
DES	Drug eluting stent
DOF	Degrees of freedom
FDA	Food and Drug Administration
FLE	Fiducial localization error
FRE	Fiducial registration error
HDL	High density lipoprotein
ICP	Iterative closest point
ITA	Internal thoracic artery
ITK	Insight segmentation and registration toolkit

LAD	Left anterior descending artery
LCO	Left coronary ostium
LDL	Low density lipoprotein
LVAp	Left ventricular apex
MARS	Monitored atherosclerosis regression study
MI	Myocardial infarction
MIDCAB	Minimally invasive direct coronary artery bypass
MPO	Myeloperoxidase
MR	Magnetic resonance
MVA	Mitral valve annulus
OPCAB	Off-pump coronary artery bypass
OR	Operating room
PCI	Percutaneous coronary intervention
PTCA	Percutaneous transluminal coronary angioplasty
RA-CABG	Robot assisted coronary artery bypass grafting
RMS	Root-mean-square
SVD	Singular value decomposition
TEE	Transesophageal echography
TRE	Target registration error
US	Ultrasound

Chapter 1

Introduction

1.1 Coronary Artery Disease

Coronary artery disease (CAD) is one of the most common diseases worldwide. In North America, CAD is the leading cause of death. For example, 44% of the mortality and much of the morbidity in the United States is attributed to CAD [1]. The average life expectancy would increase by almost 7 years if all forms of CAD were to be eliminated [2]. The costs related to cardiac disease is very high according to the 2010 National Heart, Lung and Blood Institute which reported that CAD costs patients $155.7 billion for medical care and $503.2 billion in direct and indirect economic costs [3].

Except for a small number of patients, CAD is caused by a condition called atherosclerosis, which occurs when fatty plaques or other substances are formed on the walls of arteries and restrict normal blood flow. Since fatty plaques can be caused by many different factors, there is no single cause of CAD. However, clinicians and scientists have developed a set of "risk factors" that are measurable characteristics that predict the probability of developing CAD. The next section will review some of the risk factors which predispose to developing CAD.

1.1.1 Risk Factors

1.1.1.1 Lipoproteins

It has been established that low-density Lipoprotein (LDL) and high-density Lipoprotein (HDL) cholesterol is closely linked to CAD. Increased LDL cholesterol concentration increases the risk of CAD [4–6], while reduced HDL is also an indicator of CAD [4, 7, 8]. Although the role of LDL has not been fully determined, most researchers believe that its major role is in the formation of blood clots.

1.1.1.2 Blood Pressure

Blood pressure in patients is also an important factor in developing CAD. Master et al. have reported that patients who have increased blood pressure were more susceptible to developing CAD and having a stroke [9]. Moreover, hypertension is associated with insulin resistance, which may increase the risk of atherosclerosis through other mechanisms [10].

1.1.1.3 Smoking

In a 2010 report, the latest from the U.S. Department of Health and Human Services, the Surgeon General confirmed that smoking was an independent risk factor for CAD [11]. Although it is not known exactly how tobacco increases the risk, one of the effects of smoking is the acceleration of atherogenesis, which is the formation of atherosclerosis. This indicated an increased risk for clinically manifested CAD.

1.1.1.4 Male sex

Being a male is one of the highest risk factors for CAD [12]. In the United States, one in every three men younger than 60 develops CAD, in contrast to only one in 10 for women [1]. Although middle aged males have a higher risk of CAD, this risk

increases for post-menopausal women and the rate is eventually identical for both sexes who are older than 60.

1.1.1.5 Diabetes

Beckman *et al.* [13] reported that patients with diabetes have a higher risk of developing CAD. Many patients who have diabetes develop insulin resistance and insulin resistance is found to be associated with decreased HDL cholesterol, increased LDL cholesterol, as well as increased blood pressure [14].

1.1.2 Symptoms

Symptoms of CAD can vary from totally asymptomatic to fatal. However, the most common symptom is chest pain or discomfort (angina). As atherosclerosis blocks normal blood flow in the arteries, the lack of oxygen to the heart tissue, commonly expressed as angina, is the result. Possible symptoms other than angina encompass shortness of breath, fatigue during activity, acute coronary syndrome (ACS) or sudden cardiac death. Patients with ACS are at high risk of cardiac muscle cell death in the immediate future. Possible outcomes of cardiac muscle cell death are unstable angina and myocardial infarction (MI).

1.2 Treatment Options For CAD

Below, we consider some treatment options for CAD.

1.2.1 Medication

Medication is a common option to prevent or reduce the further development in the early stages of CAD. Although many factors contribute to the progression of CAD, there are several biomarkers which indicate the severity of the disease. For example,

elevation of Myeloperoxidase (MPO) and LDL, and reduction of HDL are strong indicator of the atherosclerosis. The following section will explain the three different types of drugs which are commonly used to treat CAD : statins, beta-blockers, and antiplatelet drugs.

1.2.1.1 Statins

Statins is the common name for the group of HMG-CoA reductase inhibitors used to control HDL and LDL. As the literature reported, the development of CAD is closely related to the level of LDL in the blood stream [15]. Statins work by inhibiting an enzyme called HMG-CoA reductase, which is responsible for producing LDL. Among different cholesterol controlling drugs, statins have proven effective in reducing cardiovascular morbidity and mortality in both primary and secondary prevention. The role of primary prevention is to decrease the rate of heart attacks and strokes for those who have not had any known cardiovascular diseases. Secondary prevention refers to treatment administered to patients with pre-existing cardiovascular disease.

Waters *et al.* [16] conducted the Canadian Coronary Atherosclerosis Intervention Trial (CCAIT) and concluded that patients who have received Lovastatin (one of the statins) experienced less progression of CAD compared with those who were treated with a placebo. Another trial, Monitored Atherosclerosis Regression Study (MARS), was also consistent with the reports from CCAIT [17]. Pravastatin, a second statin, has also been shown to reduce the level of LDL. The Pravastatin Limitation of Atherosclerosis in the Coronary arteries study showed that patients who were treated with Pravastatin had a 40% reduction in LDL cholesterol level and progression of atherosclerosis, compared with the control group who received placebo [18]. Statins also have shown its effectiveness on MPO, which is an enzyme that promotes atherosclerosis and acute coronary syndromes, with Ndrepepa *et al.* [19] reporting that the use of statins lowered the level of MPO by 20% compared to patients without statin therapy.

Statins have been proven to reduce the risk of atherosclerosis through other means other than controlling cholesterol levels. For example, Bellosta *et al.* reported that the use of statins can inhibit smooth muscle cell growth. Thus, these agent may slow the progression of atherosclerosis [20]. In addition, Rosenson *et al.* showed that statins promote plaque stability through a combination of its lipid-lowering properties and inhibitory effects on macrophage activation that consequently reduces the risk of plaque rupture [21].

1.2.1.2 Antiplatelet Drug

As platelets are believed to play an important role both in the pathogenesis of atherosclerosis and in the development of coronary thrombosis, antiplatelet drugs, which inhibit the activity of platelets, are typically used on patients who have CAD, with well proven benefits.

Antiplatelet drugs were first introduced to treat CAD in 1953 for protective purposes. Although there are many different antiplatelet drugs, aspirin and clopidogrel are the ones which have been widely studied and most commonly used. The benefit of aspirin was first reported in 1763, but in order to make this drug applicable for CAD, it took much more time and it only recently became a therapy in CAD. The use of aspirin was researched both for primary and secondary prevention. Research on aspirin for secondary prevention is well studied and shows positive results in that it improves clinical outcomes in patients with ACS, coronary artery bypass grafting (CABG), and percutaneous coronary intervention (PCI) even though there is a risk of bleeding. The Antiplatelet Trialists' Collaboration conducted a study involving 135000 patients, with the following results: any serious vascular mortality was reduced by 25%, non-fatal myocardial infraction by 30%, non-fatal stroke by 25% and vascular mortality by 15% [22]. Moreover, the Canadian Antiplatelet Therapy Guideline recommends a low dose of aspirin for patients who have undergone ACS, CABG, PCI and cerebrocascular disease [23]. For primary prevention, however, the effective-

ness of antiplatelet drugs does not appear to be consistent, as some studies showed the improvement of the outcomes [24] while other studies stated otherwise [25]. Generally speaking, even with the benefits, there is major risk of bleeding from treatment with antiplatelet drugs. Therefore, benefits are rather nullified or diminished and other types of therapy are recommended.

Lastly, recent studies found that patients who have been treated with antiplatelet drugs for long time do not respond to them and such situations have been termed "aspirin or clopidogrel resistance". This phenomenon could put patients in a dangerous situation as Gum *et al.* [26] reported. Patients who have a resistance to aspirin have a higher risk of myocardial infraction and death, compared with aspirin responders. Therefore, even with the benefits of antiplatelet drugs, its use should be carefully monitored.

1.2.1.3 β-adrenergic blockers

β-adrenergic blockers are so named as they inhibit β-adrenergic receptors of epinepherine and norepinipherine on the sympathetic nervous system, which are responsible for increasing heart rate and vasocontraction. Since the β-adrenergic blocker was clinically introduced in 1962, it has been used for treating CAD and hypertension.

β-adrenergic blockers have been used as the first-line therapy for hypertension and its related diseases. For example, β-adrenergic blockers significantly reduced the risk of developing a stroke when compared with a placebo. Also, the patients who were treated with β-adrenergic blockers showed a 20% lower risk of having a cardiovascular event compared to those on a placebo [27]. As a treatment for CAD, β-adrenergic blockers are typically used for secondary prevention rather than primary prevention. Hawkins *et al.* [28] reported up to a 34% reduction in mortality with the use of β-adrenergic blockers to those patients who have had previous MI. Moreover, sudden cardiac death was also reduced by up to 16% in patients who were taking β-adrenergic blockers compared to those on a placebo [29]. With these positive clinical

outcomes, ACC/AHA guidelines recommend that patients who have had MI take β-blocker therapy unless patients show a clear contraindication to the therapy [30].

The main limitation of β-adrenergic blockers is, however, that its effectiveness on primary prevention is still not clear. Moreover, like other types of medication, the use of β-adrenergic blockers is limited to preventing the progress of the disease and to relieving the pain instead of curing the disease. These limitations force patients who have severe CAD to undergo other types of treatment such as an intravascular therapy or surgery.

1.2.2 Intravascular Therapy

Intravascular therapy is a non-surgical revascularization treatment for CAD which uses a catheter to perform arterial dilation at the site of atherosclerosis. There are two different types of PCI procedure dependent on how arterial dilation is performed: i.e. with a balloon and stent. Balloon angioplasty was invented before stent angioplasty and uses a balloon, which is placed in a catheter, to be inflated at the site of atherosclerosis. On the other hand, a stent deployment leaves a metal frame to support the arterial wall following inflation of the target vessel.

1.2.2.1 Percutaneous Transluminal Coronary Angioplasty

Percutaneous Transluminal Coronary Angioplasty (PTCA) was first performed on coronary arteries in 1977 by Dr. Andreas Gruentzig [31]. After the success of the first PTCA, it became an alternate treatment option to CABG surgery for atherosclerosis.

PTCA is a procedure used to increase the luminal size of the artery where blood flow has been disrupted by atherosclerotic plaque, so that the normal blood flow can be restored. For a typical PTCA procedure, a guide catheter containing a flexible guide wire, a balloon catheter and contrast enhancing material for visualization, is inserted into the femoral artery. Under fluoroscopic guidance, the guide catheter

advances to the ostium of the coronary artery to be dilated. Once the guide catheter reaches its destination, the guide wire continues to advance to the stenosis and is positioned in the distal arterial segment. The deflated balloon catheter then travels through the wire and is positioned across the stenosis. The location of the guide wire and the deflated balloon catheter is frequently confirmed by fluoroscopy with the aid of intravascular contrast injected via the guide catheter. Once the location of the deflated balloon catheter is confirmed, the balloon is inflated at a constant pressure (usually 6 to 8 atmospheres). If the dilation of the stenosis is adequate in the view of the surgeon, the guide catheter including the guide wire and the balloon catheter are removed. If the desired dilation is not reached, the balloon catheter may be replaced with one of larger diameter, while the guide wire continues to be held across the stenosis.

From an efficacy point of view, about 90 percent of the non-occluded coronary cases are performed successfully, which leads to effective relief of angina [32, 33]. Moreover, because of the nature of its non-invasiveness, PTCA is often considered as an alternative treatment option for patients with recurrent angina who have undergone CABG previously. However, PTCA appears less effective when the stenoses are long, eccentric, or located at the ostium or the site of a branch point [34]. Patients with unstable angina or advanced age might also have a lowered success rate.

A small percentage of patients who undergo PTCA procedures experience complications: $3\% - 5\%$ of patients have MI and $3\% - 7\%$ require emergency bypass surgery [35–37]. The death rate from PTCA is reported as $0\% - 6\%$ [38, 39] while $2\% - 7\%$ of patients experience acute or abrupt closure of the artery [36, 40]. When the artery has a abrupt closure, an immediate revascularization (PTCA or CABG) is required. For long-term complications, restenosis, the state when stenosis recurs, frequently occurs in PTCA patients. Where the balloon dilates the lumen, damage to the smooth muscle cells in the media may occur, leading to immediate platelet deposition or thrombus formation. Restenosis typically happens within six months after

the procedure and the rate of restenosis can be as high as 50% [41–43]. Restenosis can be treated with a second PTCA treatment but the incidence of restenosis after the second treatment is similar to that after the first.

When compared to medical therapy, PTCA gives patients an immediate relief from angina and greater improvement in exercise performance [33]. However, compared to medical therapy PTCA has a higher risk of MI and emergency bypass surgery [44]. Furthermore, PTCA might cause abrupt closure of the artery or restenosis. Although PTCA has the benefits of rapid and complete relief of angina, many patients are first treated with the medical therapy and proceed to PTCA or other revascularization if the medical therapy does not work.

1.2.2.2 Stents

Due to PTCA's high rate of restenosis as a result of the damage to the smooth muscle cells or elastic recoil of the lumen, an alternative intravascular therapy is the stent. The principal mechanism of a stent is almost identical to PTCA. However, the difference between the two therapies is that stents place a metal frame after the aterial dilation which is left inside the patient permanently, while PTCA uses a balloon as an one-time therapy.

Although stents were first clinically used in 1986 [45], the use of stents began to replace PTCA around 1994 [46]. Since then the use of a stent have become the primary choice for intravascular therapy, because it reduces the risk of restenosis significantly (about $25\% - 30\%$) compared to PTCA (around 50%) [47, 48]. It also reduces the risk of the immediate need of revascularization, such as a second intravascular therapy or surgery for abrupt vessel closure, since the metal frame stays inside the lumen permanently. However, because stents introduce foreign material into the human body, there is a chance the patient may develop thrombosis, the formation of a blood clot resulting from the presence of foreign material in the blood stream. Thrombosis usually leads to MI or death [49, 50]. To prevent this, patients who have undergone

stent surgery must take an antiplatelet drug for rest of their lives. Furthermore, although the rate of restenosis is greatly reduced compared to PTCA, 30% is still high and may require repeat intravascular procedures or surgery [51]. To overcome these issues, researchers have tried different types of material to replace the metal frame, such as inorganic elements (e.g. gold) or polymer (e.g. polyactic acid and fibrin) [52, 53]. These attempts slightly decreased the rate of thrombosis , but the rate of restenosis remained as high as $25\% - 30\%$.

Drug-Eluting Stents (DES) are an advanced type of stent, that was fully approved by the Food and Drug Administration (FDA) in 2003 [53]. The metal frame in DES is coated with an outer drug-loaded layer of polymer. This allows the right amount of a drug to be placed at the site of stenosis to prevent restenosis. When compared with bare-metal stent, DES shows improved results on the rate of restenosis. Moreover, the Arterial Revascularization Therapies Study (ARTS) showed that the rate of major adverse cardiac and cerebrocascular events (including MI, death, and revascularization) is significantly lower than when using a bare-metal stent (15.9% vs 31.0%) and similar to that of CABG (16.4%) [54].

Among the many drugs which are in the trial process for their effectiveness, sirolimus and taxol are currently available in clinical trials for DES. The rate of restenosis for Sirolimus-eluting stent was as low as 2.3% compared to bare metal-stent which was as high as 52.3% [55, 56]. Also, the rate of major adverse cardiac event was reduced to 5.8%, versus 28.8%, for bare-metal stent [57]. Some literature reported that Taxol-eluting stent reduced the restenosis rate to 5% from 25% for the bare-metal stent [58, 59]. Even considering that many of these studies were conducted with small sample sizes, they adequately showed the effectiveness of using DES over the bare-metal stent.

Despite the success of DES, its chief limitation is found in repeat revascularization mostly due to restenosis. Although some literature claims that the rate of restenosis for DES is as low as 5%, the rate of repeat revascularization is still high when com-

pared to CABG (29.0%, 7.9%) [60, 61]. DES on patients who have diabetes appears not to work as well as those without diabetes because the rate of stenosis and major adverse cardiac events are much higher than CABG [54].

Finally, when stents are compared to medical therapy, one study shows that there is no significant difference in the primary event rate, which includes death and MI. However, about one third of patients who have been treated with medical therapy requires revascularization due to unstable angina [62]. In conclusion, medical therapy is optimal for those with stable angina but if patients have severe ischemia burden or unstable angina, or they want to have immediate relief from their pain, stents should be considered.

1.3 Coronary Artery Bypass Surgery

CABG surgery is a surgical treatment of CAD. The chief goal of CABG is to restore normal blood flow to the affected arteries, which were occluded by atherosclerosis. CABG is a revascularization procedure, where a bypass conduits is inserted at the region distal to the site of the atherosclerosis to provide an alternative route for blood. The first successful revascularization was performed in 1957 by Bailey [63]. With the invention of cardiopulmonary bypass (CPB), which immobilizes the heart and halts its blood flow while shunting the pateint's blood to a heart-lung machine, and the coronary angiography, CABG has become a safe and solid treatment option for those who have severe symptoms.

Due to the invasiveness of the surgery, great care must be taken when considering undergoing such surgery. Patients with mild lesions are not usually recommended for the surgery but instead are recommended other types of therapy such as medical therapy or percutaneous artery intervention. Patients who have stable angina or acute coronary syndromes are typical candidates for CABG procedure. The size of the target vessel should also be more than 1.5 mm in order to maintain high patency

after surgery.

In conventional CABG, the chest of the patient is open (median sternotomy) and the bypass conduit is harvested. The Saphenous vein or internal thoracic artery (ITA) are commonly used as bypass conduits. The choice for the right conduit depends on the location of anastomosis and the number of bypass. For example, ITA is usually chosen over the saphenous vein because ITA has better patency and is free from repeat revascularization. Fitzgibbon [64] reported that CABG using the saphenous vein had 88% early vein graft patency, but decreased to 75% after 5 years and 50% after 15 years, which may lead to re-operation. On the other hand, many studies supported ITA as the choice conduit because of its long-term patency of over 90% after 10 years [65, 66]. However, if patients requires more than three grafts, the saphenous vein is usually employed after the use of both ITA (left and right).

Daement *et al.* [60] reported that there is not much difference in the rate of death, stroke or MI when CABG is compared to intravascular therapy. However, repeat revascularization was significantly higher with stents, which could lead to a significantly increased risk of adverse cardiac events. The cost of intravascular therpy was 35% lower than that of CABG and with a better comfort level for patients after the procedure, compared to CABG [67]. In conclusion, the main benefits of intravascular therapy over CABG is the cost effectiveness of the procedure and the reduced length of recovery. However, in the long run, CABG provides a clinical freedom from repeat revascularization that intravascular therapy does not guarantee.

1.3.1 Off-pump CABG

Although an optimal surgical condition for CABG is achieved by using CPB, the complications associated with the use of CPB are pulmonary, renal and neurological dysfunction, the risk of blood loss and transfusion and myocardial injury and dysfunction [68, 69]. Moreover, patients with normal ventricular function generally tolerate the use of CPB well for prolonged periods, but it could significantly increase

the peri-operative mortality and morbidity rates if used on patients with depressed ventricular function [70]. Therefore, CABG on the beating heart started to be considered something to avoid in order to prevent the adverse effects from the use of CPB.

CABG procedure with the beating heart is generally referred to as off-pump CABG (OPCAB) and typically involves median sternomy. Unlike the conventional CABG, however, a shorter incision is required for the OPCAB because it does not need access to the ascending aorta, which is needed for a CPB. Since OPCAB deals with beating hearts, greater experience with this type of surgery is necessary and patients should be carefully monitored to increase the success rate compared to a conventional CABG. Therefore, patients, for whom the use of CPB is a risk factor, are optimal candidates. Such patients include the elderly, re-operative patients, or those with renal or pulmonary dysfunction [71–73]. Although studies are limited with small sample sizes, preliminary results show that OPCAB reduces complications associated with the use of CPB. Ascione *et al.* [74] reported that blood loss was 1.6 times higher with the on-pump patients compared with the off-pump patients. Also, only 23% of patients who underwent OPCAB needed a transfusion compared with 52% of patient having the on-pump procedure. The same group showed that the myocardial function was improved on patients with OPCAB [75]. Lastly, Plomondon *et al.* [76] claimed that the off-pump mortality and complication rates decreased from 4.0% and 14% to 2.7% and 8.8% respectively, when compared with the on-pump patients.

Although OPCAB requires a surgeon with more experience and expertise, it provides an alternative for those who could not have undergone the conventional CABG with good outcomes.

1.3.2 Minimally Invasive CABG

Although OPCAB reduced the complications with the use of CPB, this type of surgery is still limited by the requirement for a median sternomony. This may

adversely affect patients with significant post-operative morbidity and discomfort. It is now therefore possible to undergo a minimally invasive approach, which avoids median sternotomy.

The first minimally invasive surgery was performed in 1967 by Kolessove, a Russian surgeon [77], who performed internal thoracic artery grafts to coronary artery anastomosis on a beating heart. However, his pioneer work was not appreciated until nearly 30 years later when it was revisited in the 1990's with improved imaging techniques. The procedure is called minimally invasive direct coronary artery bypass (MIDCAB). MIDCAB is typically defined as a surgery without median sternotomy but with small incisions between the patient's intercostal space, and its less invasiveness leads to a better post-operative function, fewer blood transfusions, a faster recovery time, and shorter lengths of hospital stay [78–80]. However, because a surgeon has only a limited view of the heart due to the small incisions, longer operating and myocardial ischemic times have been observed, as well as target vessel misidentification may occur.

1.3.3 Robot-assisted CABG

Robot-assisted CABG (RA-CABG) is a variation of the minimally invasive approach. While MIDCAB achieves a direct view of the heart from the incisions made, RA-CABG fully depends on the visualization observed thorugh the a three-dimensional stereo endoscope. Therefore, RA-CABG is also referred to as, totally endoscopic coronary artery bypass (TECAB).

The da Vinci surgical system (Intuitive Surgical Inc., Mountain View, CA), the only such system approved by the FDA, is employed in RA-CABG procedures. The da Vinci system is composed of two parts: a master console and a slave robot. While high-definition three-dimensional video visualization is offered from the endoscope, the surgeon is situated in the master console and controls the slave robotic arms remotely. At the patient table, three small incisions are made in the patient skin to

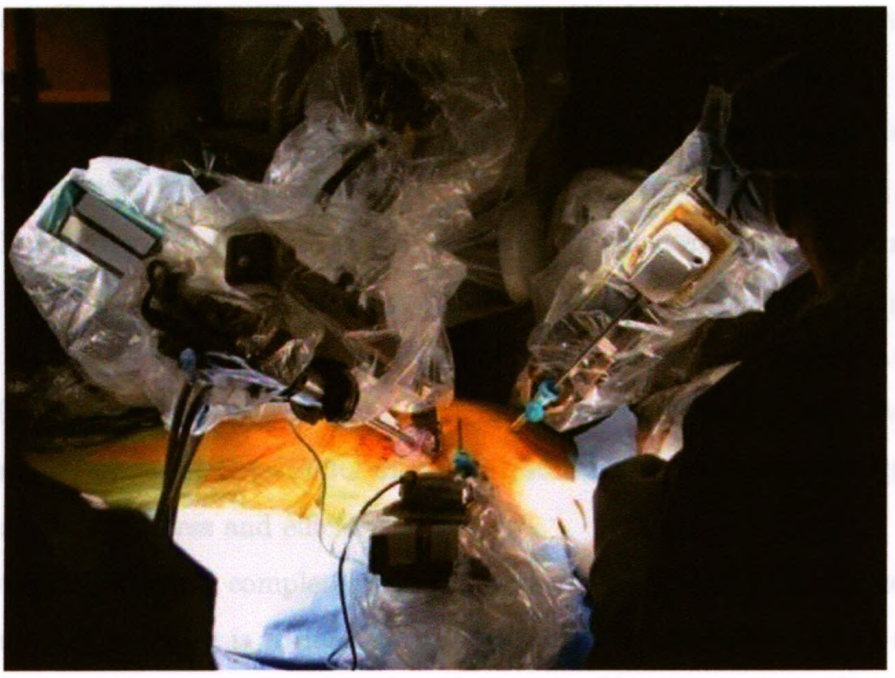

Fig. 1.1: RA-CABG of left internal mammary artery on the left anterior descending artery using da Vinci surgical system. *Image courtesy of Maria Currie, London, ON*

accomodate: the endoscope and the left and right robotic arms (**Fig. 1.1**). From there a high-definition endoscope is inserted into the thoracic cavity via the fifth intercostal space, while the third and seventh intercostals are used for the right and left robotic instruments respectively. Under the remote control of the surgeon, microsurgical instruments with 7 degrees-of freedom achieve high-precision, well-controlled and wide-ranging movement at its tips. Also, thanks to the robotic system, any unintentional movements from the surgeon are filtered.

RA-CABG can be performed either on pump, while the patient is connected to the cardiopulmonary bypass, or off-pump, on the beating heart. Although Bonatti *et al.* [81, 82] reported that all their patients recovered without any major adverse cardiac or cerebral events following the on-pump RA-CABG performed on the arrested heart, this approach may lead to complications, such as post-perfusion syndrome or arrhythmia due to prolonged use of the CPB. To minimize these risks, many groups

have adopted the off-pump RA-CABG approach [83–86], leading to approximately 25% increase in its use across North America [87].

Although off-pump RA-CABG is a new technique for revascularization, many studies have been conducted to validate its efficacy. Srivastava *et al.* [88] reported that early patency of the graft is around 99% while clinical freedom from graft failure reached 98.6%. Also, Gao *et al.* [89] concluded that RA-CABG is a safe procedure with an excellent early and midterm patency of anastomosis. Moreover, Argenziano *et al.* [90] reported that they achieved 91% of overall freedom from reintervention or angiographic failure for RA-CABG on the arrested heart, and Falk [91] agreed with the procedure's safeness and efficacy.

As surgeons depend completely on the visualization of the 3D endoscope, the experience and expetise is a must to perform a procedure safely. With the same reason, they encounter a substantial learning curve. Moreover, although the number of RA-CABG procedures are increasing, the cost of the surgical system is a major factor preventing many institutions to employ it. Lastly, because of its short history, the long term results of this procedure has yet to be validated.

1.4 Motivation

A major limitation of the robot-assisted technique is the need to convert to open-chest surgery because of the difficulties associated with the access and manipulation of closed-throacic surgery. The conversion rate has been reported to be in the range of $15\% - 25\%$ [92–94] and it has been primarily caused by the inability to access the surgical target with the robotic instruments, lack of adequate workspace inside the thoracic cavity and instrument collision.

In an effort to reduce the need for conversion, several groups have relied on exploiting the pre-operative CT images routinely acquired prior to the procedures. Figl *et al.* [95] proposed a method to "highlight" the surgical targets in the endoscopic

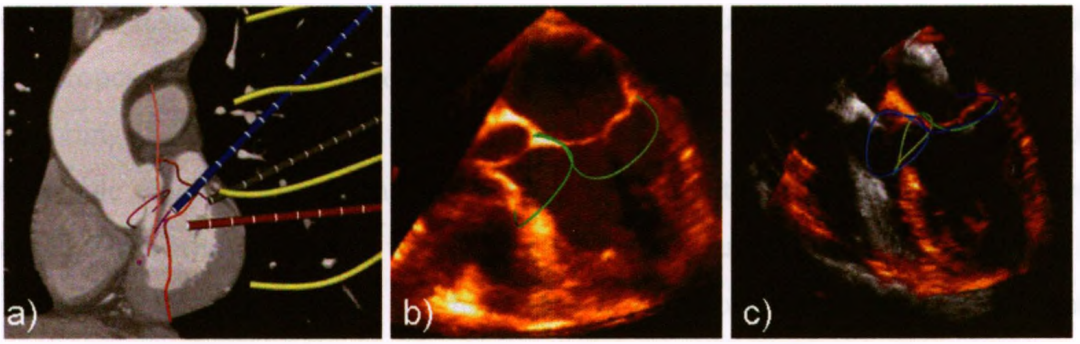

Fig. 1.2: (a) Pre-operative surgical planning based on pre-operative CT image, showing left anterior descending artery (red), robotic arms and intercostals space (yellow lines); (b) US images of left lung deflation stage with the aortic valve and mitral valve extracted; (c) The shift from left lung deflation (orange) to the thoracic insufflation (gray) and their corresponding segmented valvular structures.

display of the da Vinci system by overlaying the pre-operative CT image onto the real-time video. Unlike Figl *et al.*, who used the pre-operative image as an intra-operative image guidance tool, Trejos *et al.* [96] used the pre-procedural CT image to identify the optimal port placement configuration that facilitates access to the targets and prevents instrument collision during manipulation. To improve robustness, Falk *et al.* suggested a complete cardiac navigation platform that integrates both patient and robot modeling and surgical planning, as well as an augmented reality overlay of the pre-operative images onto the endoscopic view [97].

While these approaches rely on a surgical plan based on pre-operative data acquired days prior to the procedure, no attempts have been reported that use peri-operative information to update the pre-operative plan, to better reflect the intra-operative conditions. In order to ensure adequate space for instrument manipulation, the procedure workflow of RA-CABG comprises two "invasive" processes - left lung deflation and CO_2 thoracic insufflation (see **Fig. 1.2**). As a result, the intra-operative location of the heart and surgical targets may differ significantly from that depicted in the pre-operative CT image. Thus, by not taking into account these migration patterns, conversion may be required, as the planned access path to the target ves-

sel may be invalidated by the peri-operative heart displacement. Hartung *et al.* [98] have proposed an image-guided approach which overlays the segmented left anterior descending (LAD) artery — a typical surgical target for CABG procedures, onto the endoscopic video by registering the pre-operative CT to the intra-operative stereo image. Their study, however, was conducted via median sternotomy rather than in a minimally invasive fashion, and hence the heart displacement induced via open-chest access could exceed that induced by robot assistance. Thus, we propose a novel method for acquiring peri-operative images of the heart using tracked ultrasound (US) and predict the intra-operative location of the LAD by registering the pre-operative CT data to the intra-operative US data. This approach has the potential to provide an optimal port placement during pre-operative surgical planning and consequently reduce the conversion to conventional CABG.

1.5 Thesis Contributions

The goal of this project is to improve the pre-operative surgical planning of RA-CABG by providing peri-operative migration patterns of the LAD through US-to-CT registration. The specific objectives that must be met to achieve this goal are:

- Develop registration techniques which fuse intra-operative US images to pre-operative CT images.
- Conduct an *in vitro* validation study, in which clinically observed migration patterns were simulated to assess and compare the accuracies of the registrations
- Conduct clinical validation study using offline data from patients who underwent RA-CABG.
- Measure the shifts of the heart induced by peri-operative interventions.

1.6 Thesis Outline

This thesis is organized as follows:

Chapter 1 provided as an introduction to the clinical background of coronary artery disease to provide a context for the motivation of the work to be presented in the remainder of this thesis. The pathophysiology and the treatment of coronary artery disease as described, as well as the different types of CABG techniques.

Chapter 2 introduces image-guided surgery and its current status. It presents and discusses the registration technique, which is a crucial part of image-guided surgery. It also introduces the rigid-body registration algorithms that were developed as part of this thesis' work.

Chapter 3 is a description of the *in vitro* validation experiments performed on a beating heart phantom to assess the accuracy of the registration techniques.

Chapter 4 presents a clinical validation as well as the clinical applications of the registration. Offline patient data were employed for the clinical validation following simulations. The migration patterns of the heart, which were induced by interventions in RA-CABG, were also observed.

Chapter 5 presents conclusions and explores future directions. A discussion is presented on how the pre-operative surgical planning of RA-CABG can be enhanced by updating the migration patterns of the heart and how the registration technique can be extended into other types of cardiac surgeries.

Chapter 2

Image Registration

Since the development of the x-ray by Roentgen in 1895, medical imaging has since significantly improved and been extended for other types of imaging such as US, CT, magnetic resonance (MR) images, positron emission tomography, and single-photon emission computed tomography. Nowadays, many procedures employ more than one type of imaging modality and the role of imaging is no longer limited to finding a lesion before a procedure, but is actively employed intra-operatively to improve the outcome of the procedure, i.e., image-guided surgery. To obtain maximum benefits from multiple modalities, it is important to fuse different modalities effectively. Registration is one way to fuse images within a single frame. This chapter will review the current techniques of registration in medical imaging and the mathematical explanation of "rigid-body" registration, which was employed in our project.

2.1 Image Registration in surgeries

As explained above, imaging is used to visualize important anatomical features, either pre- or intra-operatively. However, each imaging modality has different usages during the course of the procedure. Thus it is important to show the changes in various anatomical features between different stages of the procedure within the same

modality, as well as between different imaging modalities. Image registration plays a key role in the detection of change between stages by aligning one set of images to another. US imaging is commonly used intra-operatively bacause of its unique ability to acquire images in real-time, while other modalities such as CT or MR images are typically taken in pre-operative stage. However, the lack of detail from US requires registration to CT or MR images, which provide more image details and anatomical features. Image registration from CT, MR or fluoroscopy to US has been reported by many groups such as Huang *et al.* [99] who registered 2D US to 3D CT to provide high quality details of the beating heart. Also, Gobbi *et al.* [100] overlaid intra-operative US images onto a pre-operative MR image in stereotactic neurosurgery to gain better visualization during the procedure, while Linte *et al.* [101] registered subject-specific models, segmented from MR images, to intra-operative US images in order to create a virtual reality environment for image-guided mitral valve surgery. Recently, Lang *et al.* [102] registered fluoroscopy to US images to improve visualization during percutaneous aortic valve replacement surgery.

Image registration is widely used in medical imaging research, in fields such as neurosurgery [103–106], radiotherapy [107, 108] and cardiac surgery [109–111], and many different registration algorithms such as rigid-body registration and non-rigid registration have been developed to meet the needs of the different cases outlined above. Among these different techniques, we focus solely on rigid-body registration in this thesis.

2.2 Rigid-body Registration

The rigid-body registration problem can be formally stated as an approximation problem. Given two different datasets (usually images or sets of points), rigid-body registration aligns them so that important spatial features are matched between the datasets by applying a simple transformation. While the datasets can have different

dimensions depending on images (typically 2D or 3D), rigid-body registration has six degrees of freedom (DOF) in three dimensions (3D), which specifies the translation and rotation required to align the images. Note that rigid-body registration sometimes implies registration which includes rigid-body, similarity, and affine registration. Similarity transformations comprise translation, rotation and anisotropic scaling (9 DOF), while affine transformation has an additional shearing transformation on top of the similarity transformation (12 DOF). In this thesis, "rigid-body" registration is defined to be a simple 6 DOF registration. In the following two sections, two different rigid-body registration techniques are discussed.

2.2.1 Point-based Registration

Registration algorithms use different types of constraints. The types of rigid-body registration can typically be divided into two classes, landmark-based and intensity-based. Given two image datasets, intensity-based registration does not require dataset segmentation for feature extraction, but rather uses correlation metrics on the intensity patterns in the datasets to perform the registration. Therefore, it is important to know what imaging modalities are being used prior to registration, as intensity-based registration employs different voxel measures for registration processes compared to point or feature based. Generally speaking, registration can be employed on the same modalities (intramodality) or different modalities (intermodality). For intramodality registration, the sum of the squared intensity difference can be used as a registration quality metrics, while mutual information or normalized mutual information may be preferred for intermodality registration.

In point-based registration, on the other hand, it is the identification of homologous features in each image that is important. Feature extraction can be performed manually or automatically, and the points collected are called fiducial markers or fiducial points. Once the desired anatomical features have been extracted from the datasets, the registration then discards the original datasets and proceeds with just

the point sets defining the features for further processing. While point-based registration may be performed in 2D to 3D or 3D to 3D, for the purpose of our discussion, point-based registration will refer to 3D to 3D only. Given two equal sized sets of points, p, the moving points, and q, the fixed points, point-based registration becomes the problem of finding the least squares rigid-body transformation which minimizes the Euclidean distance between the two point sets. To achieve this, one computes a translation vector, t, and a rotation matrix, R, that minimizes:

$$\varepsilon^2 = \sum_{i}^{N} |R \cdot p_i + t - q_i|^2, \tag{2.1}$$

where N is the number of points.

Pseudo code for the registration process is given below:

(1) Find the centroid (center of mass) of each data set.

$$\overline{p} = \frac{1}{N} \sum_{i=1}^{N} p_i \tag{2.2}$$

$$\overline{q} = \frac{1}{N} \sum_{i=1}^{N} q_i \tag{2.3}$$

(2) Compute the displacement between the centroid and each point in the data set.

$$\widetilde{p} = p_i - \overline{p} \tag{2.4}$$

$$\widetilde{q} = q_i - \overline{q} \tag{2.5}$$

(3) The minimization problem becomes:

$$\varepsilon^2 = \sum_{i=1}^{N} |\widetilde{q}_i - R \cdot \widetilde{p}_i|^2 \tag{2.6}$$

R can be found by minimizing ε^2 and then computing $t = \overline{q} - R\overline{p}$.

This least-squares estimation problem has a closed-form solution and so does not require an iterative solution method. Horn's method using unit quaternions [112] and a singular value decomposition (SVD) [113] is commonly used for this procedure (see **Appendix A**).

2.3 Surface-based Registration

Surface-based registration is similar to point-based registration in that it also requires feature extraction from image datasets. While point-based registration is restricted to using homologous points, which are the corresponding points on both images that should represent the same ordered features, surface-based registration has more freedom in terms of the types of constraints used because surfaces can be defined as a simple point set, faceted surface, implicit or parametric surfaces. The variety of constraint choices allows this registration to be used widely in image-to-image (CT, MR or other modalities), or physical-to-image registration (i.e., bone to image). Surface-based registration is employed when the number of homologous point pairs is insufficient for robust registration. The skin boundary surface, any bone structure or any other surfaces with high contrast are good candidates for this registration.

2.3.1 Iterative Closest Point

There are many registration algorithms available for surface-based registration, such as Head and Hat or Disparity functions. However, the iterative closest point (ICP) algorithm is one of the most widely used algorithms. ICP was first introduced by Besl and McKay [114] and finds the best transformation between two datasets by reducing the general nonlinear minimization problem to an iterative point-based registration problem. While ICP can be used in various representations as described above, point sets and triangle sets are the most common representations, since many segmentation algorithms in medical imaging extract features in this manner.

Given the source and target datasets (i.e. images), the steps involved in ICP are:

(1) An initial registration (i.e. a simple rigid body registration) is applied to the source dataset so that the two datasets align relatively close to each other.

(2) Place the source dataset into a k-dimensional (kD) tree.

(3) Each target point finds its closest Euclidean distance source point from this kD tree.

(4) Using these target and closest source point sets, perform point-based registration.

(5) Find the residual from the transformation to describe the quality of the match.

Steps 2 to 4 are repeated until the algorithm satisfies the termination criteria based on the difference between two adjacent registration residuals being smaller than some threshold (user defined). The initial transformation can be performed in many different ways, such as using several landmarks for the registration. As ICP is sensitive to the initial registration, it is important to first accurately align the source and target datasets before any processing is further done.

2.3.2 Robust Statistics

A potential problem with using the original ICP algorithm is that its accuracy may be compromised when the data contain erroneous measurements, since ICP weighs every point equally. However, since the data was obtained by a manual segmentation (the features are defined manually rather than computed), it is inevitable that it contains some points that are not as accurately aligned as others. Removing outliers during the registration process could greatly improve its accuracy and some types of robust estimator are widely employed to achieve this.

There are various different types of robust estimators and one way to characterize them is to compare the gross-error sensitivity, meaning how well a certain estimator responds to various ranges of error.

For example, the least-squares estimator has an unbounded gross-error sensitivity since it will include any point, no matter how large the errors are. This estimator,

therefore, is not suitable for outlier detection. For this reason, the gross-error sensitivity of most robust estimators is bounded, and different estimators have different means of setting the bounds on the gross error. The influence function (how outliers are weighed) is commonly used to visualize the gross-error sensitivity.

Three influence functions are shown in **Fig. 2.1**. As the above described, the least-square estimator demonstrates a linear behaviour without bound, while Lorenzian's and Tukey's biweight influence functions start decreasing the influence of outliers at a certain point. Given that different functions behave differently, a robust estimator should be chosen carefully based on the application.

Once the right estimator has been chosen, it is also important to determine the rejection point for a given dataset and a scale parameter is used to determine a proper rejection point. A standard scale parameter for a robust estimation (σ) is the median absolute deviation (MAD), as shown in Equation (2.7) below:

$$\sigma = c \cdot median_i \left\{ |x_i - median_j \left\{ x_j \right\}| \right\}. \tag{2.7}$$

The constant c is designated for optimizing a value of the estimator to a particular distribution. For example, if the distribution is a zero-mean normal distribution, constant c could be 1.4826 to cover one standard deviation of the population.

2.3.3 Robust ICP

Our robust ICP algorithm was originally adopted from Ma [115]. The principle of robust ICP is to perform weighted ICP, where the weights are determined by a robust estimator. To integrate the weights in ICP, Horn's method is preferred over SVD, because using weights in Horn's method has already been described in his algorithm (i.e. Tukey's biweight), while SVD does not provide any straightforward way to use the weights. Therefore, for each iteration of ICP, the scale of the robust estimator is computed based on residual errors of the dataset and consequently outliers are discriminated against while weights are assigned to the remaining data points. A

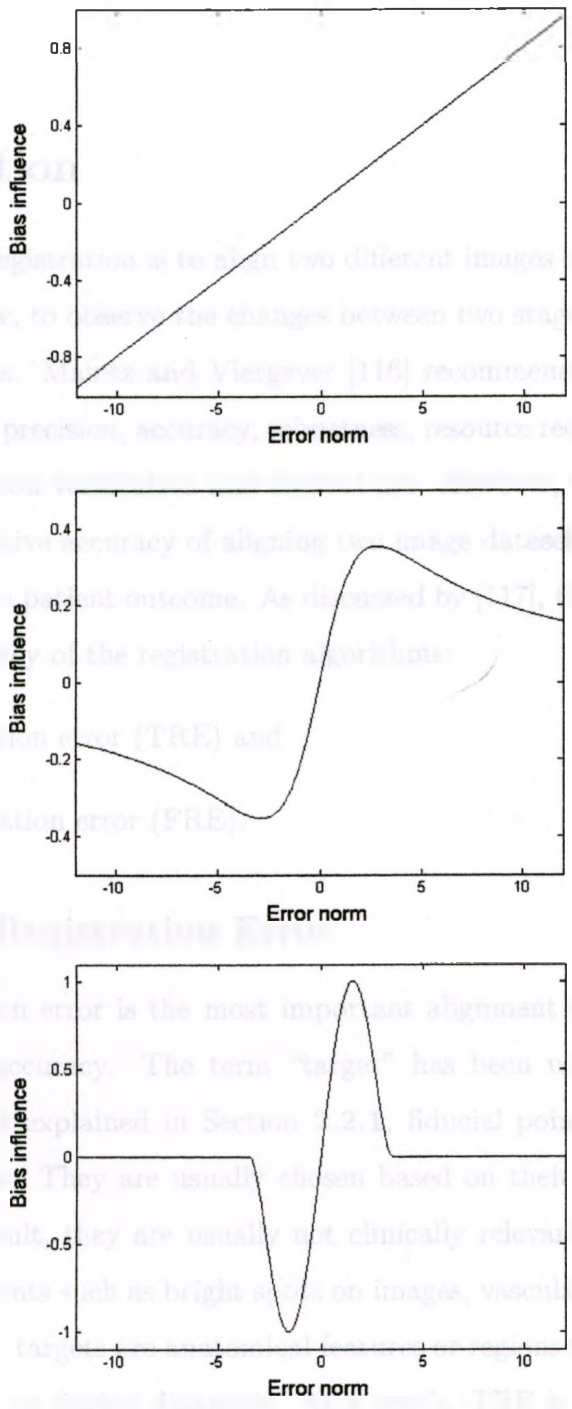

Fig. 2.1: Influence function of (a) least-squares error norm, (b) Lorentzian error norm and (c) Tukey's biweight error norm.

pseudo code for Robust ICP is provided in the **Appendix B**, which was adopted from Ma [115].

2.4 Evaluation

The purpose of registration is to align two different images of anatomical features within the same view, to observe the changes between two stages and to enhance the detail of the features. Maintz and Viergever [116] recommeneded ways to evaluate registration, such as precision, accuracy, robustness, resource requirements, algorithm complexity, assumption verification and clinical use. However, this section will focus only on the quantitative accuracy of aligning two image datasets as an assessment of reliability, and not on patient outcome. As discussed by [117], there are two measures used to define accuracy of the registration algorithms:

1. target registration error (TRE) and
2. fiducial registration error (FRE).

2.4.1 Target Registration Error

Target registration error is the most important alignment measure when speaking of registration accuracy. The term "target" has been used to differentiate it from "fiducials". As explained in Section **2.2.1**, fiducial points are those used for registration purposes. They are usually chosen based on their visibility in different modalities. As a result, they are usually not clinically relevant anatomical features but rather salient points such as bright spots on images, vascular junctions etc. However, unlike fiducials, targets are anatomical features or regions the surgeon is looking for in the procedure or during diagnosis. As a result, TRE is the most meaningful of the error measurements. Given that p and q represent target points in the first and second image datasets respectively, TRE can be found using T, a transformation

computed from evaluating a registration:

$$TRE = ||T(p) - q||^2. \tag{2.8}$$

2.4.2 Fiducial Registration Error

Fiducial registration error is a measurement based on the points which have no significant clinical meaning, but are used for registration only. When fiducials are defined either manually or automatically, there may be errors associated with localizing them. This type of error is called fiducial localization error (FLE) and because FLE always occurs before registration is performed, FLE affects both the FRE and TRE. The presence of FLE means that FRE cannot be used as an estimate of TRE because it may cause either an underestimation and an overestimation of FRE. Underestimation occurs when a value of FRE is lower than the value of TRE. This happens because a registration attempts the best to find the best transformation to match the fiducials. When actual fiducials are incorrectly defined in the same manner in one image dataset, it will yield low FRE because the registration tries to align fiducials as close as possible. However, this will lead TRE to be greater since the error in localizing fiducials adds onto the TRE. For example, if the FLE on one image dataset is 1 mm in the x direction while the FLE on another dataset is 2 mm in the y direction, the registration would result in a FRE of 0 but a TRE of 2.2 mm ($\sqrt{1^2 + 2^2} \approx 2.2$) because of the FLE (see **Fig. 2.2**).

Secondly, overestimation occurs when the value of FRE is higher than the value of TRE, when the error on each fiducial is not defined in the same manner to each other, but with a different magnitude and/or direction. The end result could be that TRE is small after the registration but FRE would be larger compared to TRE, which concludes that FRE overestimates TRE. For example, half of the fiducials have an error of +1 mm in the x direction while the other half have an error of -1 mm in the x direction. In this case, FRE will yield 1 mm while TRE will continue to be zero

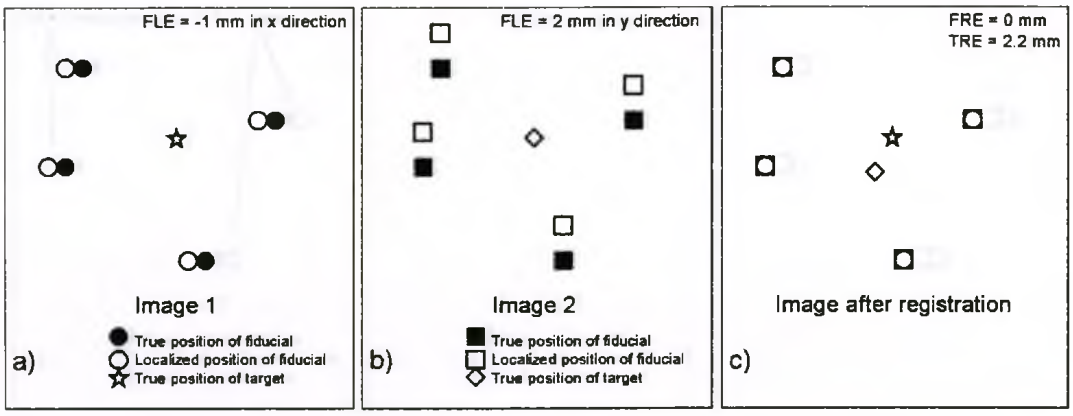

Fig. 2.2: Schematic of underestimation: (a) Fiducials are localized with FLE of -1 mm in x direction on the first image, (b) Fiducials are localized with FLE of 2 mm in the y direction on the second image and (c) registration yields 0 mm of FRE while 2.2 mm of TRE due to underestimation

(see **Fig. 2.3**). Lastly, Fitzpatrick [118] has shown that TRE and FRE are actually uncorrelated mathematically and experimentally via computer simulation. Although FRE values are much less than TRE in general, FRE could still be a good measure to evaluate the registration results because FRE is easier to compute than TRE and measuring FRE could be a good means of validating the quality of the registration.

FRE is typically reported as a root-mean-square (RMS) calculation as follows:

$$FRE^2 = \sum_{i}^{N} |T(p_i) - q_i|^2 . \tag{2.9}$$

2.5 Summary

As different modalities are being used in an image guided surgery, it is crucial to have a good registration between source and target image datasets. This chapter explained rigid-body registration, with a focus on landmark based registration. While there are many types of rigid-body registrations available, our work focuses on a modified ICP algorithm, which is a type of surface-based registration which uses Tukey's biweight statistical estimator. Moreover, we have discussed the evaluation

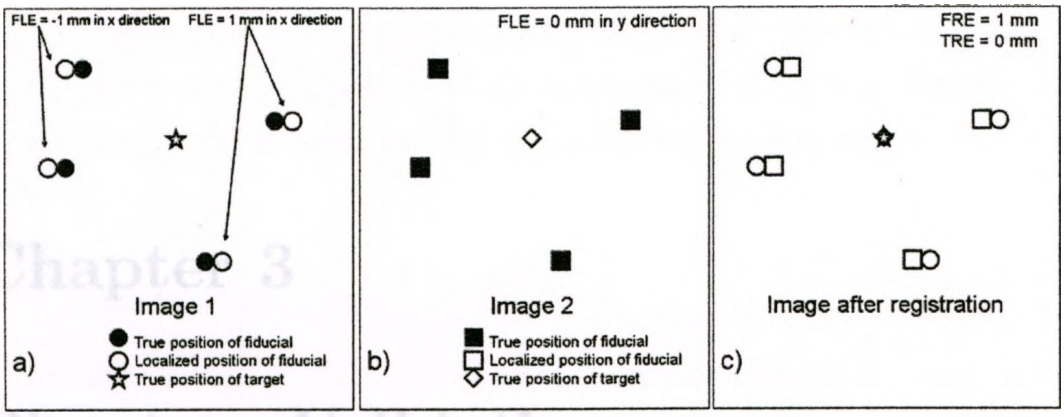

Fig. 2.3: Schematic of overestimation: (a) Half of the fiducials are localized with FLE of -1 mm in the x direction while others are localized with FRE of 1 mm in x direction on the first image, (b) Fiducials are localized with FLE of 0 mm on the second image and (c) registration yields 1 mm of FRE while 0 mm of TRE due to overestimation.

measures (TRE and FRE) to assess the accuracy of the registration. The following chapters explore how the registration discussed in this chapter may be implemented in image-guided robot assisted CABG procedures.

Chapter 3

Phantom Validation

3.1 Introduction

As discussed in the motivation of the project, the intra-operative imaging modality (i.e. 2D Trans-esophageal echocardiography) is not able to identify the surgical target vessel under the current RA-CABG setting. To bypass this issue, registrations that involves the anatomical features as contraints, which are visible on both pre-op CT and intra-op Trans-esophageal echocardiography (TEE), were developed. As a initial step toward a full validation, we conducted an *in vitro* study using a realistic heart model.

3.2 Materials and Methods

3.2.1 Clinical Procedure Workflow

In a typical robot-assisted CABG procedure, a pre-operative CT image of the patient is acquired for surgical planning (Stage_{CT}). To ensure sufficient work space inside the closed-chest, during the procedure, the patient undergoes several "interventions" consisting of intubation and anesthesia delivery (Stage_0), deflation of the

left lung ($Stage_1$), and thoracic insufflation ($Stage_2$). To illustrate how pre- and intra-operative imaging is used to obtain measurements of the heart migration during the RA-CABG procedure, we follow a hypothetical patient through the proposed workflow.

3.2.1.1 Image Acquisition

A cardiac-gated CT image of the patient's thorax depicting the heart at mid-diastole is acquired as part of a routine pre-operative exam for a patient undergoing RA-CABG. Since the images are acquired with contrast enhancement, they provide reliable information with regards to the shape and location of the major vessels, including the LAD.

During the robot-assisted procedure, 2D TEE is used to acquire images of the patient's heart at each stage of the peri-operative workflow using a Philips SONOS 7500 scanner(Philips, Andover, MA). While TEE is the standard imaging modality for cardiac monitoring during interventions, for this application, the image acquisition is spatially tracked using a modified TEE transducer [119]. Surgical tracking technology has become indispensable in image-guided interventions, as it allows surgeons to identify the position and orientation of the instruments and visualize them relative to the anatomy and surgical targets. In spite of the high localization accuracy achieved using optical tracking technology [120], this application favours magnetic tracking since no direct line-of-sight can be established between the TEE probe inserted in the patient's esophagus and an optical tracking camera mounted overhead. As a result, the NDI Aurora (Northen Digital Inc., Waterloo, ON, Canada) magnetic tracking system is employed; the TEE transducer is tracked via a 6 DOF sensor embedded inside the casing of the probe, while another 6 DOF single disc marker is attached to the patient as reference. Using the magnetically tracked probe, US images of the patient's heart are acquired from different views to depict several features of interest at each peri-operative workflow stage.

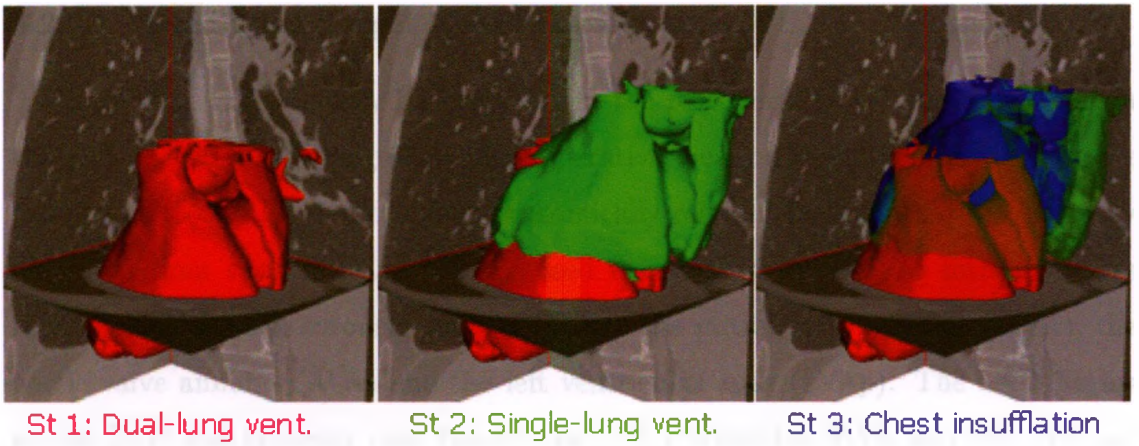

Fig. 3.1: Graphical representations of the peri-operative heart shift during RA-CABG procedure: (a) after intubation and anaesthesia (red) (b) after left lung deflation (green), and (c) after chest insufflation with CO_2 (blue)

3.2.2 Estimating Peri-operative Heart Migration

In a previous investigation [109], the migration of the heart was studied in four patients using a feature-based registration technique that relied on the mitral and aortic valve annuli to describe the location of the heart. Preliminary data have shown that the heart undergoes substantial displacement following lung deflation and thoracic insufflation, resulting in changes in position on the order of $25 - 35$ mm between the pre- and intra-operative conditions (**Fig. 3.1**).

We also have observed from the same study that the morphology of the valvular structures (i.e. length of short and long axis, valve annulus perimeter and inter-valvular distance) remains relatively unchanged throughout the workflow, despite considerable displacement of the heart. Based on the suggested conclusions that no significant non-rigid deformations occurred, our aim is to improve the currently-employed feature-based rigid registration by adding additional constraints near the base and apex of the heart, to yield optimal alignment along the surgical target - the LAD coronary vessel.

3.2.2.1 Predicting Target Vessel Location

Since the LAD can only be identified in the pre-operative CT image and not in the peri-operative US images, its intra-operative location must be inferred from the pre-operative data. Therefore, four anatomically relevant features that can be easily identified from both CT and US are used to assist in the pre- to intra-operative registration: the left coronary ostium (LCO), the mitral valve annulus (MVA), the aortic valve annulus (AVA) and the left ventricular apex (LVAp). The LAD begins at the LCO and typically runs toward the LVAp, while the MVA and the AVA are located on either side of the staring point of the LAD. The MVA and the LVAp are captured from a mid-esophageal-4-chamber-view at 20° increments from 0° to 180°, while the AVA and the LCO are viewed from five long axis view images with 10° increments, and one short axis view of the aorta at 30°. These features are manually defined by an expert anesthetist on both CT and US images using a custom-developed feature extraction tool: the MVA and the AVA are delineated as rings while the LCO is identified as a point, and the LVAp as a paraboloid. Lastly, the path of the LAD is also traced on the pre-operative CT dataset.

3.2.2.2 Pre- to Intra-operative Feature-based Registration

Two rigid-body registration algorithms that employ the four anatomical features were investigated in this work: the first treats the extracted features as single landmarks with empirically-assigned weighting factors, while the second relies on a modified ICP approach to align the four features in the homologous datasets.

Weighted Landmark-based Registration: After the four anatomical features — the LCO, MVA, AVA and LVAp — are identified in the pre- and peri-operative datasets, as a means to reduce the variability associated with their manual segmentation, the features are treated as single landmarks, as follows: the LCO, the centroids of the mitral (MVA) and aortic (AVA) valve annuli, and the vertex (i.e.global mini-

mum) of the LVAp segmented surface. Moreover, treating these features as landmarks had the added benefit of reducing processing time.

Simple landmark-based registration was performed using the four landmarks, followed by the minimization of the Euclidean distance between the LCO and LVAp using downhill simplex optimization [121]; these two features — LCO and LVAp, were selected as the primary constraints for the registration given they bound the superior and inferior ends of the LAD.

Robust ICP-based Registration: The second registration technique employed the complete geometry of the anatomical features consisting of the LCO, two 3D closed curves describing the MVA and AVA, and a parabolic structure defining the "cap" of the left ventricular apex. For better accuracy, a virtual surface model of the left ventricle apex was generated from the pre-operative CT dataset along with the intra-operative features.

The robust ICP-based approach is an extension of the traditional ICP algorithm employing Horn's method to compute the registration transform [112, 114], with the addition of a robust estimation technique [115]. The purpose of the robust estimator is to reduce the effect which outliers within the datasets — in this case resulting from inconsistencies in the extracted features due to manual segmentation — may have on the overall registration. Based on different robust estimators which were discussed in **2.3.2**, Tukey's biweight is the best option for our project as it is considered to provide reasonable performance across a wide range of three-dimensional data [115]. The robust estimator assigns weights to each point based on the residual error between the registered source and target points after each iteration, and it also effectively discriminates against outliers whose residual error exceed a certain value by assigning them zero weights [122]. The estimated weights are then used in Horn's method to compute the transform.

3.2.3 *In vitro* Experimental Validation

3.2.3.1 Experimental Apparatus

The *in vitro* study was conducted on a heart phantom (The Chamberlain group, Great Barrington, MA, USA) and the apparatus was set up in a similar configuration to that observed in the operating room (OR). Heart migration patterns similar to those observed in our preliminary clinical study [109], were simulated *in vitro* by changing the position and orientation of the phantom to mimic the observed peri-operative displacements. Sixteen CT-visible fiducials were attached to the surface of the heart phantom: ten were used to perform the physical-to-image space registration and the remaining six were used to outline the LAD path (**Fig. 3.2a**). The position of the heart phantom was tracked throughout the experiment using a 6-DOF NDI magnetic sensor attached to the phantom, while another 6 DOF single disc marker was rigidly attached to the table to serve as global reference.

3.2.3.2 Image Acquisition

A pre-operative CT image of the phantom was acquired on a GE 64-slice Light-Speed VCT scanner with the voxel size of 0.49 mm x 0.49 mm x 0.63 mm (General Electric, Milwaukee, WI, USA) and a virtual model of the phantom was generated using automatic segmentation tools available in ITK [123].

Peri-operative US images of the phantom were acquired using the magnetically tracked TEE probe described in **3.2.1**. The position and orientation of the phantom was changed twice to simulate the lung deflation and thoracic insufflation; the four features - LCO, MVA, AVA and LVAp - were imaged three times at each of the three workflow stages, and also the entire protocol was repeated three times to minimize human error.

Once all the images were collected, the features were extracted using a custom-developed segmentation tool. All features were defined in the same 3D coordinate

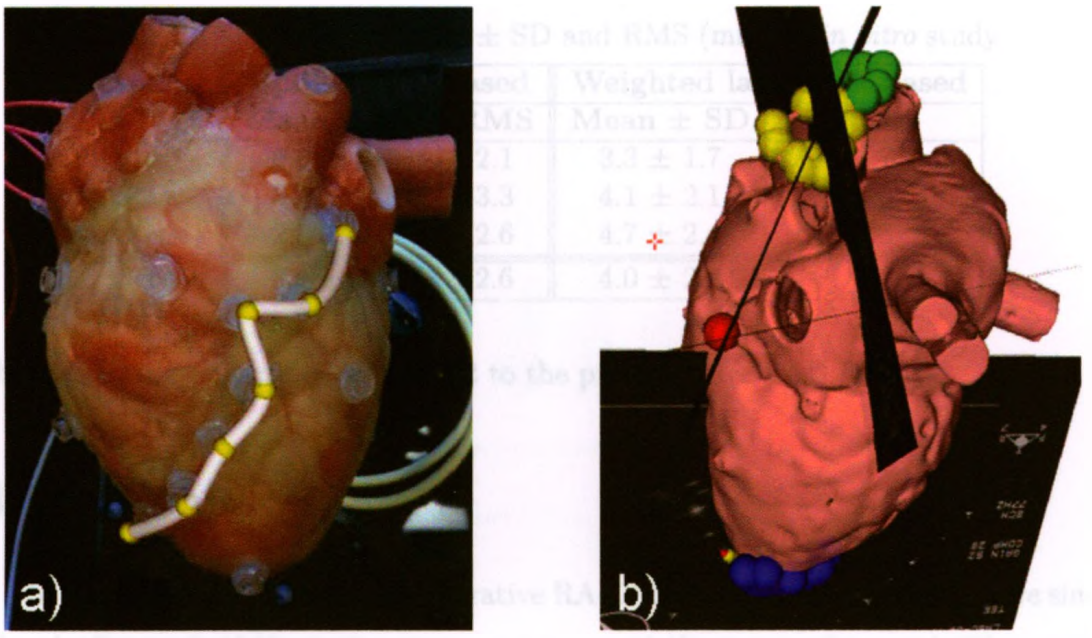

Fig. 3.2: (a) An heart phantom image showing the LAD path; and (b) Peri-operative US image acquisition protocol showing imaging of the apex and coronary ostia using incrementally tracked 2D US images.

space: the LCO was identified as a single marker, the MVA and AVA were segmented as 3D "rings", and the LVAp was segmented by manually tracking the epicardial contours of the apex in each of the 2D US images (**Fig. 3.2**). Lastly, the location of the LAD vessel was also delineated on the pre-operative CT image using the six fiducial markers, while its peri-operative location would be inferred using the proposed registrations techniques.

3.2.3.3 Computing LAD Target Registration Error

The six fiducials that marked the LAD path were used to assess the TRE between the predicted LAD location and its gold-standard location at each stage in the workflow. The gold-standard locations of the LAD fiducials were determined by recording their positions at each stage using a magnetically tracked pointer. The predicted LAD location was identified by applying the registration transform computed from

Table 3.1: LAD TRE: Mean ± SD and RMS (mm) in *in vitro* study

Stages to CT	Robust ICP-based		Weighted landmark-based	
	Mean ± SD	RMS	Mean ± SD	RMS
$Stage_0$	2.0 ± 0.7	2.1	3.3 ± 1.7	3.7
$Stage_1$	3.0 ± 1.2	3.3	4.1 ± 2.1	4.6
$Stage_2$	2.5 ± 0.8	2.6	4.7 ± 2.4	5.3
Overall	2.4 ± 1.0	2.6	4.0 ± 2.2	4.6

the registrations described in **3.2.2.2** to the pre-operative LAD fiducials.

3.3 Results

In this experiment, three peri-operative RA-CABG procedure workflows were simulated. For each of these nine poses, we acquired three sets of tracked US images, defined the features of interest and used the two different proposed registration algorithms (weighted landmark-based registration and robust ICP-based registration) to predict the intra-operative LAD vessel location based on its pre-operative location. The TRE between the actual locations of the LAD target fiducials (the ground truth) and their predicted locations from the registration were computed for each of the stages ($Stage_0$, $Stage_1$ and $Stage_2$) in the pre-operative CT images (**Fig. 3.3**). **Table 3.1** summarizes the overall TREs computed from two registrations between the three stages. We can see the robust ICP-based registration outperforms weighted landmark-based registration at all stages. Also, for a visual interpretation of the LAD TRE, **Fig. 3.4** shows the virtual model of the heart phantom along with the gold-standard and predicted LAD paths of robust ICP-based and landmark-based registration.

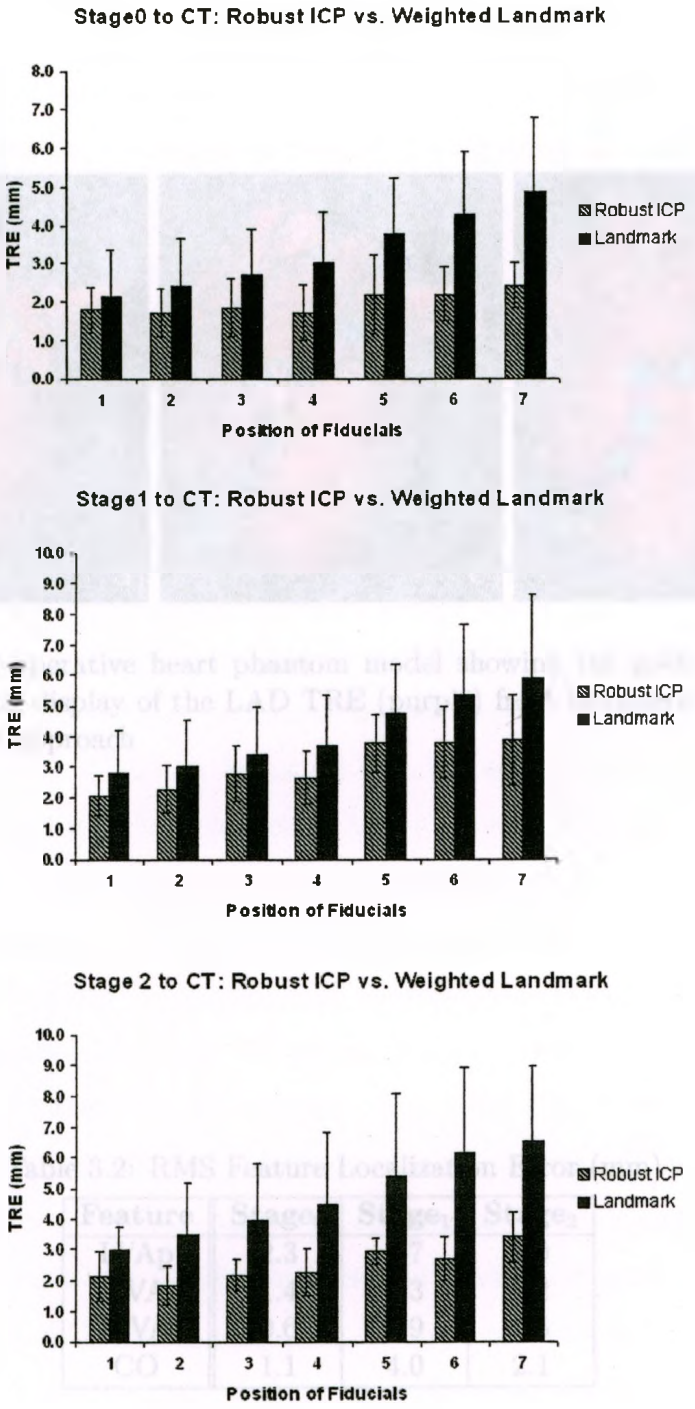

Fig. 3.3: Graphical representation of the target registration errors of the two registration techniques (robust ICP-based and Weighted Landmark-based) from perioperative stages (Stage_0, Stage_1 and Stage_2) to pre-operative stage (Stage_{CT}).

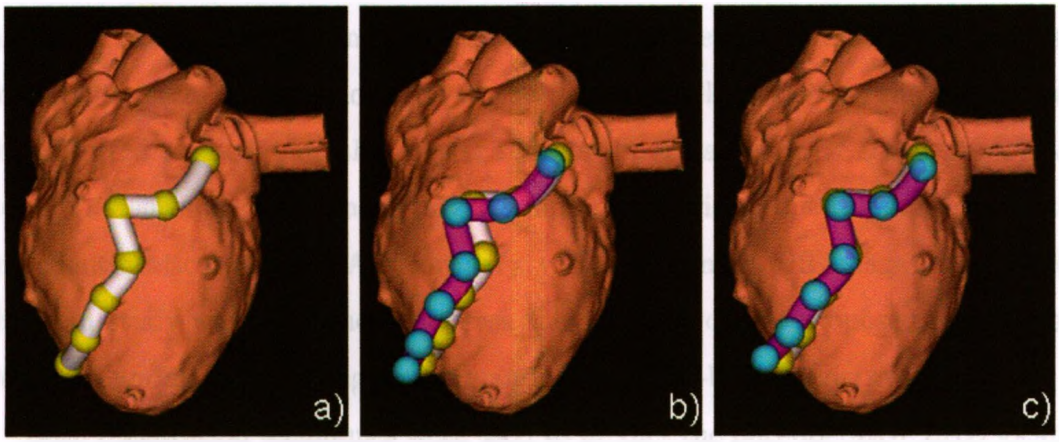

Fig. 3.4: (a) Pre-operative heart phantom model showing the gold-standard LAD (white); (b) Visual display of the LAD TRE (purple) from landmark-based, (c) and robust ICP-based approach

Table 3.2: RMS Feature Localization Error (mm)

Feature	**Stage$_0$**	**Stage$_1$**	**Stage$_2$**
LVAp	2.3	4.7	4.0
AVA	1.4	1.3	1.2
MVA	0.6	1.9	1.5
CO	1.1	4.0	2.1

3.4 Discussion

This work constitutes the first steps towards optimizing pre-operative planning for RA-CABG procedures. Motivated by a recent clinical study that revealed substantial migration of the heart during the peri-operative procedure workflow, our goal is to predict the intra-operative location of the target vessel, to provide the surgeon with an optimized surgical plan that better reflects the intra-operative stage. As a bridge to the *in vivo* validation, considering the limitations arising due to poor visualization and identification of the LAD coronary vessel in clinical US images, the *in vitro* phantom study was performed to assess the accuracy of two proposed registrations: weighted landmark-based registration and robust ICP-based registration.

Both registration techniques were used to predict the peri-operative LAD location at each pose in the workflow; according to the TRE computed along the LAD, the robust ICP-based approach outperformed the landmark-based approach, leading to an overall RMS TRE of 2.6 mm versus 4.6 mm, respectively (see **Table 3.1**). From the results, the trend of higher errors closer to the apical end of the LAD was observed in the weighted landmark-based registration while the robust ICP-based registration stays relatively consistant. This observation is mainly due to the nature of the registration as the weighted landmark-based approach was limited to the use of four landmarks for registration, while the robust approach used the complete geometry of the features of interest for registration. The RMS FRE between the predicted location of four features and the gold-standard location from CT was computed, and **Table 3.2** includes a summary of the RMS localization error assoicated with the identification of each of the four features used to drive the weighted landmark-based registration: LCO, LVAp, MVA and AVA. As observed, the point-based localization of the LVAp and the LCO was consistently challenging, mainly due to the 2D nature of the US images used to identify a 3D structure and the development of the robust ICP-based registration minimized the inconsistency of the point localization

very well.

Nevertheless, considering that the anastomosis is performed two thirds of the way from the left coronary ostium toward the apex, the RMS TRE on point 5 were 2.7 mm and 4.5 mm for the robust ICP-based and the weighted landmark-based approach respectively. While the clinically tolerable error is on the order of 10-15 mm, the accuracy provided by the proposed techniques is well within the allowable boundaries in the *in vitro* experimental setting.

3.5 Conclusions

Driven by the clinical motivation to improve the pre-operative planning of RA-CABG procedures, here we have proposed and evaluated two registration techniques used to predict the intra-operative target vessel locations. Our techniques were validated in an *in vitro* study simulating the clinically-observed RA-CABG procedure workflow. The robust ICP-based registration yielded a 2.6 mm RMS TRE while the weighted landmark-based registration yielded 4.6 mm, suggesting that the use of the full extent of the selected features led to a better accuracy and consistancy in predicting the LAD location. As the validation is limited to the *in vitro* study, our technique is needed to be evaluated in more clinical setting in order to strengthen its validity to be used clinically.

Chapter 4

Clinical Application and Validation

4.1 Introduction

Although the *in vitro* study provided a good evaluation of the accuracy of the registration algorithm, the apparatus was still deemed inadequate in ensuring that the study fully simulated an actual RA-CABG. Therefore, there was a need to perform another validation study in a clinical setting. This chapter presents a validation study based on the offline patient data which were acquired from RA-CABG procedure.

4.2 Materials and Methods

As a follow-up of the *in vitro* validation, a clinical validation was conducted for further assessment of the registration. Although there is a limitation that the target vessel is not identifiable in US images, *in vivo* animal experiments involve complex interventions such as lung deflation and chest insufflation which might cause premature loss of the subject prior to the end of the procedure. Therefore, a validation study was conducted using offline data acquired from four patients who had undergone RA-CABG and the Monte Carlo simulation method was used to estimate the maximum TRE at the LAD.

4.2.1 Image Acquisition

For each patient, a pre-operative CT and three-stage peri-operative US images were acquired as described in **3.2.1.1**. A pre-operative CT was acquired prior to the RA-CABG surgery as a routine of the patient care as well as for the pre-operative surgical planning purpose. During the surgery, three different interventions to the patients have been made to ensure an adequate workspace inside the chest cavity — Stage_0 - after intubation and anaesthesia, Stage_1 - after left lung deflation, Stage_2 - after chest insufflation. A magnetically tracked TEE was employed to acquire the anatomical features of the heart at each stage of the interventions. Following image acquisition, the four anatomical features were extracted by an expert anaesthetist, while LAD was segmented only from CT image. Like the feature extraction in the *in* vitro study, the AVA and the MVA were delineated as "ring" while the LCO was delineated as a single point. The apical region was extracted as a paraboloid shape which consists of a cloud of the points. Peri-operative features at each stage were registered to the pre-operative stage by robust ICP-based registration, which was shown to be superior to the landmark-based registration approach.

4.2.2 Assessing Target Vessel Location

For the *in vitro* study, the accuracy of the proposed registration algorithms in predicting the intra-operative LAD vessel location was assessed as the TRE computed along the LAD. However, since the gold-standard location of the LAD could not be identified from the US images, we resorted to computing the FRE of the features of interest and conducting a series of simulations to estimate the TRE at the LAD based on the FRE computed above.

Given that the LAD branches off at the left coronary ostium and toward the apex of the heart, in the simulation study, the displacement of the LAD was constrained by the displacement of these two features. As the FRE of these features were computed,

the maximum TRE at the LAD can be estimated and assessed against the clinically tolerable error (10-15 mm).

4.2.2.1 Simulation Study

A simulation study was conducted using the Monte Carlo method. The shape of the LAD was delineated from each patient's CT data and the vessel was defined as 14 sequential points (**Fig. 4.1a**). For peri- to pre-operative stage registration, the computed maximum FRE of the LCO and LVAp was used as boundary conditions for the simulations. The displacement for the superior end of the LAD (closely located to the LCO) was bounded by the maximum FRE of the LCO, while the displacement for the inferior end of the LAD (closest to the LVAp) was constrained by the maximum FRE of LVAp. The peri-operative migration patterns of the LAD were modeled as a rigid-body transformations consisting of a translation and rotation component. Since the purpose of this study was to estimate the "maximum" TRE at the LAD, the translation was randomly generated, while ensuring both ends of the LAD were inelastically constrained at the maximum boundaries set by the FRE at the LCO and LVAp. Considering the curvature of the LAD across the surface of the heart, the rotation component was approximated as a rotation about an axis defined by the superior and inferior ends of the LAD with a ramdonly generated angle within a range of 30 degrees (**Fig. 4.1b**).

4.2.3 Measuring Changes in Heart Position

Following the clinical validation, the migration patterns of the heart during RA-CABG were measured. As the LAD is not visible on intra-operative US images, it is not feasible to measure the shift of the LAD directly. Therefore, with the assumption that the heart does not deform significantly during the RA-CABG procedure and the heart is treated as a rigid structure, the migration paterns of the whole heart would

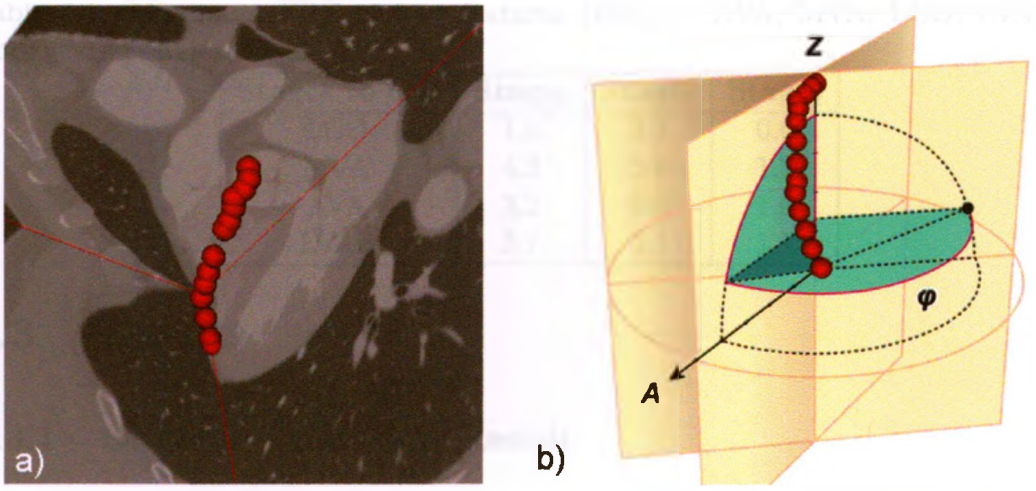

Fig. 4.1: (a) LAD extracted from patients CT data (b) LAD with the axes of rotation.

be a good estimate of that of the LAD.

Prior to the registration, three stages of intra-operative US images as well as pre-operative CT images were acquired. US images are then transferred into the CT image space by aligning homologous features identified during the first peri-operative dataset (Stage_0) and the pre-operative dataset (Stage_{CT}). These two stages are physiologically equivalent, considering the same patient position and dual-lung ventilation, and therefore minimal anatomical variations are expected between them. As a result, heart displacement induced by the interventions can be measured with respect to the principal body axes in the CT coordinate system. The robust ICP-based registration was employed to corresponding source and target images to estimate the displacements of the heart at each stage (Stage_1 and Stage_2) from its original location (Stage_0).

Table 4.1: Maximum FRE of four features (mm) — AVA, MVA, LCO, LVAp — employed in clinical validation

Stages to CT	$Stage_0$	$Stage_1$	$Stage_2$
LCO	1.6	3.1	0.6
MVA	4.3	5.6	1.7
AVA	3.2	6.0	1.6
LVAp	3.7	5.1	1.1

4.3 Results

4.3.1 Clinical Validation Result

We conducted a clinical validation based on the offline patients data to validate the proposed registration in a more clinically representative fashion. Pre-operative CT and peri-operative US images of four patients undergoing RA-CABG were acquired and the AVA, MVA, LCO and LVAp were extracted. The robust ICP-based registration was employed to register the peri-operative stages to their pre-operative couterpart. **Table 4.1** summarizes the overall FRE of the features employed in the registration.

Moreover, the results of simulation study are shown in **Fig. 4.2**. The simulations were conducted using the Monte Carlo method and were used to estimate the TRE at the LAD following the peri- to pre-operative registration, using the maximum FRE of LCO and LVAp respectively. A total of $10,000$ runs was conducted for each simulation.

4.3.2 Result of Measuring Heart Shift

The result is based from six patients who underwent RA-CABG procedure. **Table 4.2** showed the magnitude of the displacement of the heart during interventions — $Stage_0$ - after intubation, $Stage_1$ - after left lung deflation, $Stage_2$ - after chest insufflation, with respect to the principal body axes in the CT coordinate system. Also, **Fig. 4.3** gave the graphical representation of these changes.

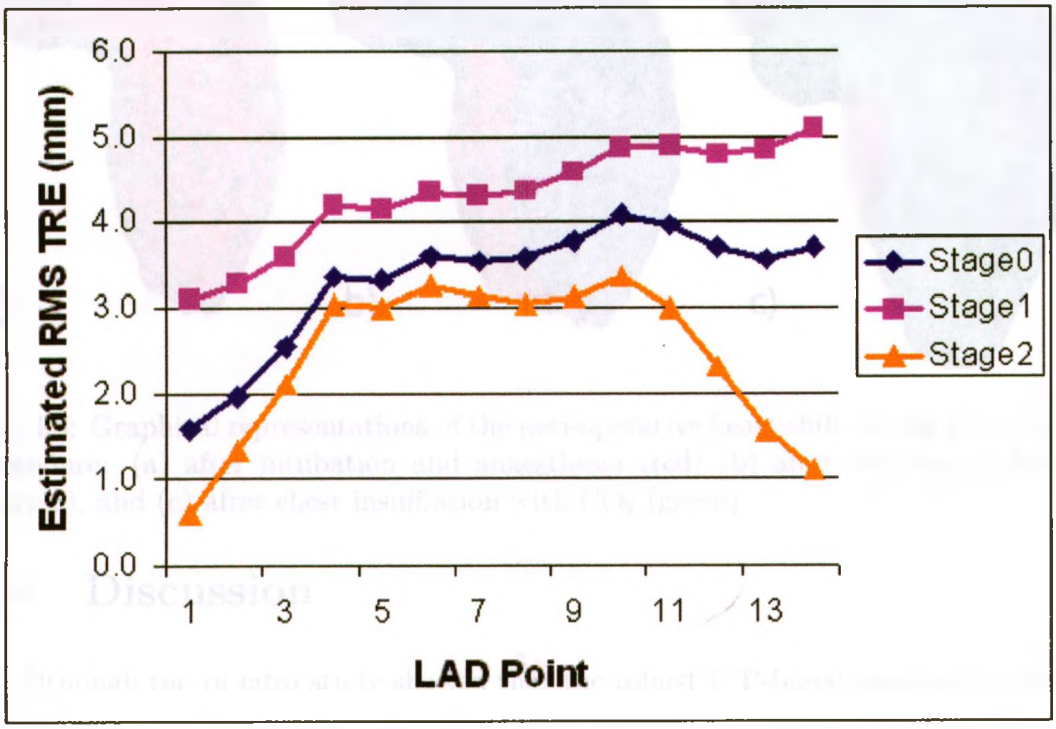

Fig. 4.2: Estimated RMS TRE of the LAD from Monte Carlo simulations which were conducted for each peri-operative stage

Table 4.2: Displacement of the heart with respect to the principal body axes in the CT coordinate system for Stage_0 to Stage_1, Stage_0 to Stage_2, Stage_1 to Stage_2 (mm)

Workflow	**Stage$_0$ to Stage$_1$**	**Stage$_1$ to Stage$_2$**	**Stage$_0$ to Stage$_2$**
Left/Right	14.3	−4.4	12.8
Anterior/Posterior	−1.4	9.3	11.9
Superior/Inferior	0.4	−6.4	1.3
overall	14.4	12.1	17.5

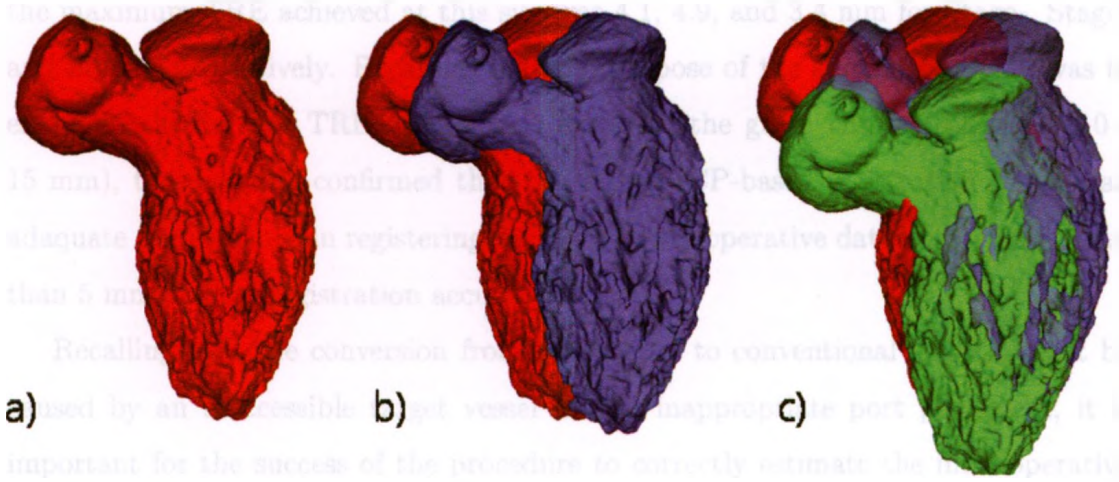

Fig. 4.3: Graphical representations of the peri-operative heart shift during RA-CABG procedure: (a) after intubation and anaesthesia (red) (b) after left lung deflation (purple), and (c) after chest insufflation with CO_2 (green)

4.4 Discussion

Although the *in vitro* study showed that the robust ICP-based registration yields a reasonable peri- to pre-operative registration accuracy, its performance still needs to be evaluated in a more clinically relevant scenario. As a result, patient data acquired during four RA-CABG patients were used for another validation study. The major limitation of clinical data is that the target vessel cannot be identified due to the poor image quality of the peri-operative US images, which in turn impedes the estimation of the TRE between the predicted and true target vessel. To bypass this issue, a simple Monte-Carlo method simulation was conducted. The LAD is anatomically bounded by the LCO at its superior end and the LVAp at its inferior end. Since the FRE of these features can be estimated from the registration, these values were used to constrain the maximum displacement of the LAD at its two ends during the simulation. For each peri-operative stage, the maximum TRE of the LAD was estimated through the simulation which is shown in **Fig. 4.2**. Considering the typical anastomosis site is located two thirds of the way along the LAD from its superior end,

the maximum TRE achieved at this site was 4.1, 4.9, and 3.4 mm for $Stage_0$, $Stage_1$ and $Stage_2$, respectively. Recalling that the purpose of the simulation study was to examine whether the TRE of the LAD exceeded the given clinical tolerance (10 - 15 mm), these results confirmed that the robust ICP-based registration provide an adaquate performance in registering the peri- to pre-operative dataset, yielding a less than 5 mm clinical registration accuracy.

Recalling that the conversion from RA-CABG to conventional CABG might be caused by an inaccessible target vessel due to inappropriate port placement, it is important for the success of the procedure to correctly estimate the intra-operative location of the heart. Since there has not been any literature reported related to the migration patterns of the heart during RA-CABG, our preliminary results provide a glimpse of intra-operative heart motion detection which needs to be further investigated. The displacements of the heart were observed in terms of principal body axis from the starting location ($Stage_0$) to stages after each interventions ($Stage_1$ and $Stage_2$) as shown in **Table 4.2**. A big shift, 14.3 mm, to the left was observed from $Stage_0$ to $Stage_1$ because of the collapse of left lung deflation. Once the chest is insufflated with CO_2, the heart was shifted 9.3 mm to anterior, 4.4 mm to right and 6.4 mm to inferior in 3D space. Thus, the overall displacements from $Stage_0$ to $Stage_1$ and $Stage_2$ were measured as 14.4 mm and 17.5 mm respectively. Although this is a preliminary result from six patients, the overall displacements could be noteworthy because it showed that the heart could be shifted more than one intercostal space during peri-operative interventions, which might impact on the selection of the port placement based solely on the pre-operative CT. Therefore, it may assist in selecting an appropriate port placement if the estimatation of the heart shift could be updated into the pre-operative surgical planning.

4.5 Conclusions

This chapter evaluated the system which registers intra-operative US images into pre-operative CT images using the robust ICP-based algorithm as well as Monte Carlo simulations in a clinical validation. The results demonstrated a maximum estimated TRE within 5.0 mm at the site of anastomosis, which is within the clinically allowable error for the intended application. Moreover, they document the migration patterns of the heart, induced by left lung deflation and chest insufflation during the procedure with displacements of 14.4 mm and 17.5 mm from the starting position to position after left lung deflation and chest insufflation, respectively.

Although the system satisfies clinical needs, limitations remain which need to be overcome in order for this system to be implemented in the actual RA-CABG procedures. These will be discussed in the next chapter. Nevertheless, the work presented in this chapter is a step forward towards port placement optimization in RA-CABG procedures and may eventually lead to a reduction in the number of conversions to conventional open thoracic surgery for RA-CABG procedures.

Chapter 5

Conclusions and Future Research

In the sections below we sumarize the thesis contributions, give conclusions and point to future research possibilities.

5.1 Contributions

Much research has been conducted to overcome a chief limitation of off-pump RA-CABG, which is the conversion to median sternotomy. However, most of this work has tried to solve the problem at the pre-operative stage with the pre-operative CT scan, thus not taking into account any peri-operative changes of the heart. Because the patient undergoes two interventions, left lung deflation and subsequent chest insufflation, to ensure an adaquate space inside the thoracic cavity peri-operatively, the peri-operative shifts of the heart should be monitored and be taken into account during pre-operative surgical planning.

The work presented in this thesis contributes to the first step towards investigating the peri-operative motions of the heart during off-pump RA-CABG procedure. Magnetically tracked TEE was employed to acquire images of the heart peri-operatively while CT was acquired pre-operatively. The typical target vessel for off-pump RA-CABG is the LAD but identification of this target vessel using TEE often failed due

to the limited depth penetration of TEE probe. Therefore, registrations using four anatomical features, i.e. the weighted landmark-based and the robust ICP-based registrations, were developed to register peri-operative stage images into pre-operative stage images. These algorithms enable the displacement of the target vessel or heart to be visualized at each intervention during the RA-CABG procedure. To evaluate the registrations, an *in vitro* as well as clinical validations were conducted. In the *in vitro* study, the beating heart phantom with six fiducals that trace the path of the LAD was employed while the offline data from patients who underwent off-pump RA-CABG were used in the clinical validation. Bearing in mind that the peri-operative location of the target vessel cannot be found using current imaging modalities, simulations were run to deduce the maximum TRE of the LAD following the clinical validation.

Since two validation studies yielded positive results, the displacements of the heart at each intervention were estimated. These results show that the heart migrated more than one intercostal space for both interventions and suggest that this peri-operative shift of the heart should not be ignored during the pre-operative planning stage but rather should be adapted in order to achieve a better procedural outcome.

5.2 Future Direction

In the subsections below we describe some avenues for future work.

5.2.1 Measuring heart deformation

The project described in this thesis has been conducted based on the assumption that the heart does not deform significantly during the procedure with Linte *et al.* [109] reporting that the valvular structures of the heart did not deform much during off-pump RA-CABG. It still, however, raises questions both from clinicians and researchers about the degree of deformation of the whole heart during the procedure,

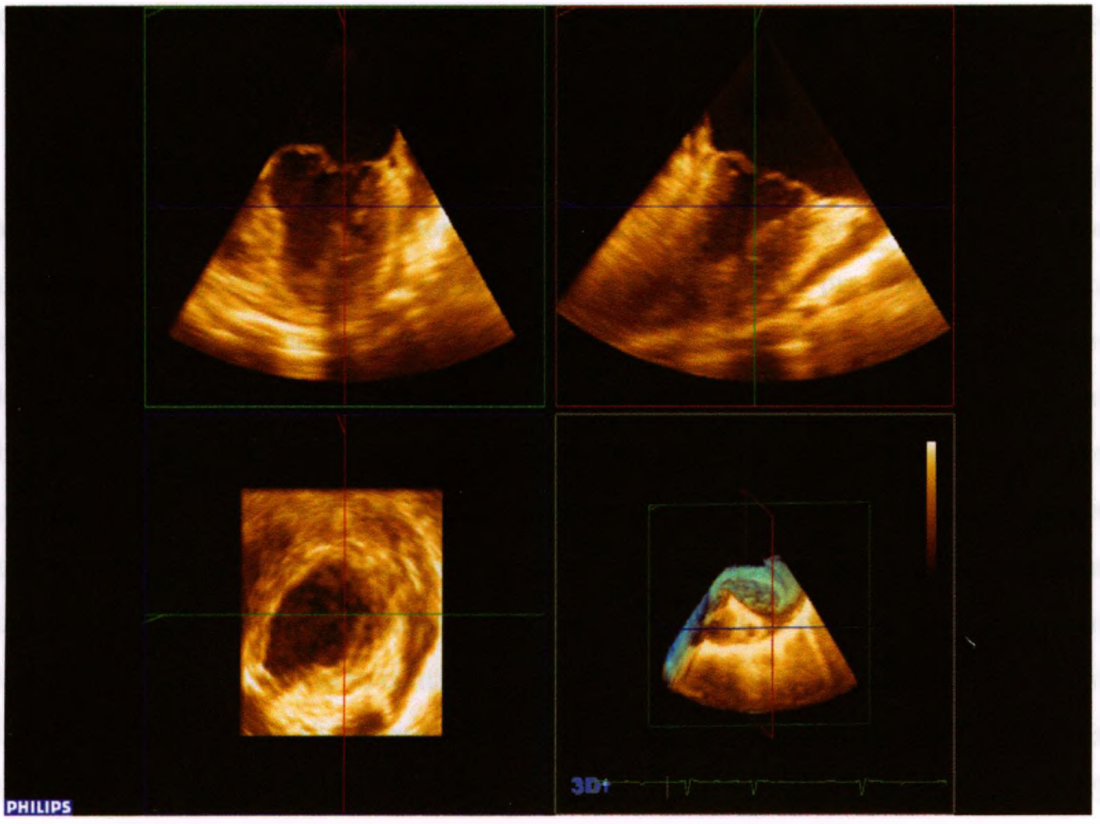

Fig. 5.1: Standard 2D view and 3D rendered view of the heart using Philips real time 3D TEE transducer and iE33 scanner

yet it has not been reported in any studies.

To examine the peri-operative deformation of the heart, the only available imaging modality currently used in the OR is the intra-operative TEE. However, the probe employed in our project was limited with its 2D dimensionality, therefore the wall of the left ventricle was not displayed well, which is a crucial landmark in order to see the deformation. Since iE33 ultrasound (Philips, Andover, MA) provides a 3D visualization, it can be used to acquire the images of the heart at each stage of the intervention in RA-CABG (**Fig. 5.1**).

Once the degree of deformation is measured, it can then be integrated with the registration to compute a more accurate displacement of the target vessel during off-pump RA-CABG.

5.2.2 Update migration patterns of the heart into the pre-operative surgical planning

From a broader perspective, this work is aimed at improving surgical planning, as well as reducing the conversion to conventional open thoracic surgery by better predicting the intra-operative location of the LAD during the pre-operative planning stage, so that an optimal port placement can be identified. Since the intra-operative locations of the LAD should be updated in the pre-operative stage, the TEE cannot be used to find its locations and they have to be "predicted" based on the pre-operative CT. The prediction of the location of the LAD could be accomplished using a statistical atlas. An atlas is a set of CT images that incorporates different information. In our case, an atlas consists of CT images of patients who underwent the RA-CABG procedures to contain the heart migration patterns and intra-operative LAD locations. Since the migration pattern would be different because of the sex, shape of rib cage or weight, it is important to select an appropriate subset of CT images from the atlas for the best results. Therefore, when a new patient undergoes the RA-CABG procedure, the CT images of the patient are acquired so as to select the right subset of CT according to a specific classification from CT atlas, similar to the one employed by Aljabar *et al.* [124].

Once a patient specific subset is constructed, the intra-operative surgical target location can be "predicted" by registering this subset of the atlas to the patient's CT scan.

5.2.3 Real-time update of the location of the target vessel

Another way to find the optimal port placement in a RA-CABG procedure is to provide a real-time update of the location of the target vessel. However, under the current protocol of RA-CABG, the US image acquisition at each pose in the workflow is conducted during the procedure, while all feature identification and registration is

performed off-line. Although registration can be performed in nearly real-time, the major drawback is feature extraction, which takes several minutes to complete, leading to difficulties in segmenting the required features in real time during a procedure. To perform real-time registration, automated feature segmentation is necessary and our lab is currently working on the development of automatic segmentation techniques for the left ventricle and valvular structures. When accurate registration is followed by the ability to perform automatic segmentation in real-time, the updated location of the target vessel can be fused into the 3D stereo endoscopic camera in the da Vinci surgical system to find an optimal port placement.

5.2.4 Extension to other types of surgery

The techniques presented in this thesis could be employed in other types of minimally invasive cardiac surgeries. Minimally invasive mitral valve repair and atrial septal defect repair are potential procedures in which this technique could be used. While off-pump RA-CABG has two interventions, such as left lung deflation and chest insufflation, mitral valve repair and atrial septal defect repair require only lung deflation (mitral valve repair - left lung, atrial septal defect repair - right lung). The target feature for mitral valve repair is the mitral valve annulus, while the septum should be identified for atrial septal defect repair. Since those features are already identified as anatomical features in our technique or can be easily identified, the proposed technique can be implemented into these two cardiac surgeries to provide an updated intra-operative location of the surgical target for the surgeon, to achieve a better procedural outcome.

5.3 Conclusion

Since the first successful revascularization surgery was performed in 1957, CABG has evolved to improve the efficacy, as well as the safety of the procedure. RA-

CABG is a very recent technology which minimizes the invasiveness of CABG and reduces the patient's discomfort during the procedure in addition to length of hospital stay. Because this technology is new and still results in a substantial conversion to conventional open-thoracic CABG, more research must be conducted in order to adopt RA-CABG as a primary treatment option for patients who need revascularization surgery. We hope that the work described in this thesis may contribute to improving the outcome of the RA-CABG procedure.

Appendix A

Solutions for least-square estimation problem

A.1 Singular value decomposition

Algorithm 1 SVD solution

1: $H =$ sum of $\widetilde{p}\,\widetilde{q}$

2: $U\Lambda V^T$ is the SVD of H

3: $X = VU^T$

4: **if** determinant of $X = 1$ **then**

5: $R = X$

6: **end if**

A.2 Horn's method using unit quaternions

Algorithm 2 Horn's method using unit quaternions

$$W = \begin{bmatrix} Sxx + Syy + Szz & Syz - Szy & Szx - Sxz & Sxy - Syz \\ Syz - Szy & Sxx - Syy - Szz & Sxy + Syx & Szx + Sxz \\ Szx - Sxz & Sxy + Syx & Syy - Sxx - Szz & Syz + Szy \\ Sxy - Syx & Szx + Sxz & Syz + Szy & Szz - Sxx - Syy \end{bmatrix}$$

Where

$Sxx = \text{sum}\left(p_{(i,1)}q_{(i,1)}\right)$

$Sxy = \text{sum}\left(p_{(i,1)}q_{(i,2)}\right)$

$Sxz = \text{sum}\left(p_{(i,1)}q_{(i,3)}\right)$

$Syx = \text{sum}\left(p_{(i,2)}q_{(i,1)}\right)$

$Syy = \text{sum}\left(p_{(i,2)}q_{(i,2)}\right)$

$Syz = \text{sum}\left(p_{(i,2)}q_{(i,3)}\right)$

$Szx = \text{sum}\left(p_{(i,3)}q_{(i,1)}\right)$

$Szy = \text{sum}\left(p_{(i,3)}q_{(i,2)}\right)$

$Szz = \text{sum}\left(p_{(i,3)}q_{(i,3)}\right)$

$V =$ eigenvectors of W

$m =$ eigenvector corresponding to maximum eigenvalue

if the largest value of $m < 0$ **then**

$m = m * -1$

end if

$$R = \begin{bmatrix} m_1^2 + m_2^2 - m_3^2 - m_4^2 & 2(m_2m_3 + m_1m_4) & 2(m_2m_4 - m_1m_3) \\ 2(m_2m_3 - m_1m_4) & m_1^2 + m_3^2 - m_2^2 - m_4^2 & 2(m_3m_4 + m_1m_2) \\ 2(m_2m_4 + m_1m_3) & 2(m_3m_4 - m_1m_2) & m_1^2 + m_4^2 - m_2^2 - m_3^2 \end{bmatrix}$$

Appendix B

Pseudo code for Robust ICP

Algorithm 3 Robust ICP using Tukey's biweight

P = source points

Q = target points

S = scale

$\{z_i\}$ = set of residual errors between P and X

$\rho_{old} = \infty$

$\rho_{new} = \sum_i \rho(z_i)$

while $|\rho_{new} - \rho_{old}| > tolerance$ **do**

$\varsigma = \text{med}\{z_i\} * 1.4826$

if $|z_i| \leq \varsigma + \text{med}\{z_i\}$ **then**

$w_i(z) = \left[1 - (z/(\varsigma + med|z_i|))^2\right]^2$

else

$w_i(z) = 0$

end if

use $P, X, \{w_i\}$ and Horn's method to find a new R and t

$newP = R(P) + t$

$\{z_i\}$ = set of residual errors between newP and X

$\rho_{old} = \rho_{new}$

$\rho_{new} = \sum_i \rho(z_i)$

end while

SPRINGER LICENSE
TERMS AND CONDITIONS

Sep 08, 2011

This is a License Agreement between Daniel S Cho ("You") and Springer ("Springer") provided by Copyright Clearance Center ("CCC"). The license consists of your order details, the terms and conditions provided by Springer, and the payment terms and conditions.

All payments must be made in full to CCC. For payment instructions, please see information listed at the bottom of this form.

License Number	2743720714239
License date	Sep 07, 2011
Licensed content publisher	Springer
Licensed content publication	Springer eBook
Licensed content title	Predicting Target Vessel Location for Improved Planning of Robot-Assisted CABG Procedures
Licensed content author	Daniel S. Cho
Licensed content date	Sep 21, 2010
Type of Use	Thesis/Dissertation
Portion	Figures
Author of this Springer article	Yes and you are the sole author of the new work
Order reference number	
Title of your thesis / dissertation	Estimating Target Vessel Location on Robot-Assisted CABG using Feature-based CT to US Registration
Expected completion date	Sep 2011
Estimated size(pages)	95
Total	0.00 CAD
Terms and Conditions	

Introduction
The publisher for this copyrighted material is Springer Science + Business Media. By clicking "accept" in connection with completing this licensing transaction, you agree that the following terms and conditions apply to this transaction (along with the Billing and Payment terms and conditions established by Copyright Clearance Center, Inc. ("CCC"), at the time that you opened your Rightslink account and that are available at any time at http://myaccount.copyright.com).

Limited License
With reference to your request to reprint in your thesis material on which Springer Science and Business Media control the copyright, permission is granted, free of charge, for the use indicated in your enquiry. Licenses are for one-time use only with a maximum distribution equal to the number that you identified in the licensing process.

This License includes use in an electronic form, provided it is password protected or on the university's intranet, destined to microfilming by UMI and University repository. For any other electronic use, please contact Springer at (permissions.dordrecht@springer.com or permissions.heidelberg@springer.com)

The material can only be used for the purpose of defending your thesis, and with a maximum of 100 extra copies in paper.

References

[1] T. Gordon and W.B. Kannel. Premature mortality from coronary heart disease. *JAMA: The Journal of the American Medical Association*, 215(10):1617, 1971.

[2] J.E. Williams, M. Massing, W.D. Rosamond, P.D. Sorlie, and H.A. Tyroler. Racial disparities in chd mortality from 1968-1992 in the state economic areas surrounding the aric study communities. *Annals of epidemiology*, 9(8):472–480, 1999.

[3] D. Lloyd-Jones, R.J. Adams, T.M. Brown, M. Carnethon, S. Dai, G. De Simone, T.B. Ferguson, E. Ford, K. Furie, C. Gillespie, et al. Heart disease and stroke statistics–2010 update: a report from the american heart association. *Circulation*, 121(7):e46, 2010.

[4] J.W. Gofman, M. Hanig, H.B. Jones, M.A. Lauffer, E.Y. Lawry, L.A. Lewis, G.V. Mann, F.E. Moore, F. Olmsted, and J. Yeager. Evaluation of serum lipoprotein and cholesterol measurements as predictors of clinical complications of atherosclerosis: report of a cooperative study of lipoproteins and atherosclerosis. *Circulation*, 14(4):689, 1956.

[5] K. Berg. A new serum type system in manthe lp system. *Acta Pathologica Microbiologica Scandinavica*, 59(3):369–382, 1963.

[6] G. Dahlen, K. Berg, and MH Frick. Lp (a) lipoprotein/pre-β1-lipoprotein, serum lipids and atherosclerotic disease. *Clinical Genetics*, 9(6):558–566, 1976.

[7] G.J. Miller and N.E. Miller. Plasma-high-density-lipoprotein concentration and development of ischaemic heart-disease. *The lancet*, 305(7897):16–19, 1975.

[8] A.R. Sharrett, CM Ballantyne, SA Coady, G. Heiss, PD Sorlie, D. Catellier, and W. Patsch. Coronary heart disease prediction from lipoprotein cholesterol

levels, triglycerides, lipoprotein (a), apolipoproteins ai and b, and hdl density subfractions: The atherosclerosis risk in communities (aric) study. *Circulation*, 104(10):1108, 2001.

[9] A.M. Master, S. Dack, and H.L. Jaffe. Age, sex and hypertension in myocardial infarction due to coronary occlusion. *Archives of Internal Medicine*, 64(4):767, 1939.

[10] S. MacMahon, R. Peto, R. Collins, J. Godwin, J. Cutler, P. Sorlie, R. Abbott, J. Neaton, A. Dyer, and J. Stamler. Blood pressure, stroke, and coronary heart disease* 1:: Part 1, prolonged differences in blood pressure: prospective observational studies corrected for the regression dilution bias. *The Lancet*, 335(8692):765–774, 1990.

[11] U.S. Department of Health and Human Services. *2010 Surgeon General's Report - How Tobacco Smoke Causes Disease: The Biology and Behavioral Basis for Smaking-Attributable Disease*, 2010.

[12] H.C. McGill and M.P. Stern. Sex and atherosclerosis. *Atheroscler Rev*, 4:157–242, 1979.

[13] J.A. Beckman, M.A. Creager, and P. Libby. Diabetes and atherosclerosis. *JAMA: the journal of the American Medical Association*, 287(19):2570, 2002.

[14] G.M. Reaven. Pathophysiology of insulin resistance in human disease. *Physiological reviews*, 75(3):473, 1995.

[15] J.R. Downs, M. Clearfield, S. Weis, E. Whitney, D.R. Shapiro, P.A. Beere, A. Langendorfer, E.A. Stein, W. Kruyer, and A.M. Gotto. Primary prevention of acute coronary events with lovastatin in men and women with average cholesterol levels. *JAMA: the journal of the American Medical Association*, 279(20):1615, 1998.

[16] D. Waters, L. Higginson, P. Gladstone, B. Kimball, M. Le May, S.J. Boccuzzi, and J. Lesperance. Effects of monotherapy with an hmg-coa reductase inhibitor on the progression of coronary atherosclerosis as assessed by serial quantitative arteriography. the canadian coronary atherosclerosis intervention trial. *Circulation*, 89(3):959, 1994.

[17] D.H. Blankenhorn, S.P. Azen, D.M. Kramsch, W.J. Mack, L. Cashin-Hemphill, H.N. Hodis, L.W.V. DeBoer, P.R. Mahrer, M.J. Masteller, L.I. Vailas, et al. Coronary angiographic changes with lovastatin therapy: the monitored atherosclerosis regression study (mars). *Annals of internal medicine*, 119(10):969, 1993.

[18] B. Pitt, G.B. Mancini, S.G. Ellis, H.S. Rosman, J.S. Park, and M.E. Mcgovern. Pravastatin limitation of atherosclerosis in the coronary arteries (plac i): reduction in atherosclerosis progression and clinical events. *Journal of the American College of Cardiology*, 26(5):1133–1139, 1995.

[19] G. Ndrepepa, S. Braun, A. Schomig, and A. Kastrati. Impact of therapy with statins, beta-blockers and angiotensin-converting enzyme inhibitors on plasma myeloperoxidase in patients with coronary artery disease. *Clinical Research in Cardiology*, pages 1–7, 2010.

[20] S. Bellosta, N. Ferri, L. Arnaboldi, F. Bernini, R. Paoletti, and A. Corsini. Pleiotropic effects of statins in atherosclerosis and diabetes. *Diabetes Care*, 23:B72, 2000.

[21] R.S. Rosenson and C.C. Tangney. Antiatherothrombotic properties of statins. *JAMA: the journal of the American Medical Association*, 279(20):1643, 1998.

[22] M. Catalano. Collaborative overview of randomised trials of antiplatelet therapy-i: Prevention of death, myocardial infarction, and stroke by prolonged

antiplatelet therapy in various categories of patients. antiplatelet trialists' collaboration. *BMJ: British medical journal*, 1994.

[23] A.D. Bell, A. Roussin, R. Cartier, W.S. Chan, J.D. Douketis, A. Gupta, M.E. Kraw, T.F. Lindsay, M.P. Love, N. Pannu, et al. The use of antiplatelet therapy in the outpatient setting: Canadian cardiovascular society guidelines executive summary. *Canadian Journal of Cardiology*, 27(2):208–221, 2011.

[24] De Gaetano. Low-dose aspirin and vitamin e in people at cardiovascular risk: a randomised trial in general practice. collaborative group of the primary prevention project. *Lancet*, 357(9250):89, 2001.

[25] P.M. Ridker, N.R. Cook, I. Lee, et al. A randomized trial of low-dose aspirin in the primary prevention of cardiovascular disease in women. *Obstetrical & gynecological survey*, 60(8):519, 2005.

[26] P.A. Gum, K. Kottke-Marchant, P.A. Welsh, J. White, and E.J. Topol. A prospective, blinded determination of the natural history of aspirin resistance among stable patients with cardiovascular disease* 1. *Journal of the American College of Cardiology*, 41(6):961–965, 2003.

[27] C.S. Wiysonge, H. Bradley, B.M. Mayosi, R. Maroney, A. Mbewu, L.H. Opie, and J. Volmink. Beta-blockers for hypertension. *Cochrane database of systematic reviews (Online)*, (1):CD002003, 2007.

[28] C.M. Hawkins, D.W. Richardson, and P.S. Vokonas. Effect of propranolol in reducing mortality in older myocardial infarction patients. the beta-blocker heart attack trial experience. *Circulation*, 67(6 Pt 2):I94, 1983.

[29] L.M. Friedman, R.P. Byington, R.J. Capone, C.D. Furberg, S. Goldstein, E. Lichstein, et al. Effect of propranolol in patients with myocardial infarction

and ventricular arrhythmia. *Journal of the American College of Cardiology*, 7(1):1–8, 1986.

[30] S.C. Smith Jr, J. Allen, S.N. Blair, R.O. Bonow, L.M. Brass, G.C. Fonarow, S.M. Grundy, L. Hiratzka, D. Jones, H.M. Krumholz, et al. Aha/acc guidelines for secondary prevention for patients with coronary and other atherosclerotic vascular disease: 2006 update: endorsed by the national heart, lung, and blood institute. *Circulation*, 113(19):2363, 2006.

[31] A. Gruntzig. Transluminal dilatation of coronary-artery stenosis. *Lancet*, 1(8058):263, 1978.

[32] A.R. Gruentzig, SB King 3rd, M. Schlumpf, and W. Siegenthaler. Long-term follow-up after percutaneous transluminal coronary angioplasty. the early zurich experience. *The New England journal of medicine*, 316(18):1127, 1987.

[33] A.F. Parisi, E.D. Folland, and P. Hartigan. A comparison of angioplasty with medical therapy in the treatment of single-vessel coronary artery disease. *Journal of Cardiopulmonary Rehabilitation and Prevention*, 12(3):213, 1992.

[34] T.J. Ryan, D.P. Faxon, RM Gunnar, J.W. Kennedy, S.B. King, et al. Guidelines for percutaneous transluminal coronary angioplasty. a report of the american college of cardiology/american heart association task force on assessment of diagnostic and therapeutic cardiovascular procedures (subcommittee on percutaneous transluminal coronary angioplasty). *Circulation*, 78(2):486, 1988.

[35] R.K. Myler, R.E. Shaw, S.H. Stertzer, T.T. Bashour, C. Ryan, H.S. Hecht, and D.C. Cumberland. Unstable angina and coronary angioplasty. *Circulation*, 82(3 Suppl):II88, 1990.

[36] M.J. Cowley, G. Dorros, S.F. Kelsey, M. Van Raden, and K.M. Detre. Acute

coronary events associated with percutaneous transluminal coronary angioplasty. *The American Journal of Cardiology*, 53(12):C12–C16, 1984.

[37] J.D. Talley, WS Weintraub, GS Roubin, JS Douglas Jr, HV Anderson, EL Jones, DC Morris, HA Liberman, JM Craver, and RA Guyton. Failed elective percutaneous transluminal coronary angioplasty requiring coronary artery bypass surgery. in-hospital and late clinical outcome at 5 years. *Circulation*, 82(4):1203, 1990.

[38] C.A. Herzog, J.Z. Ma, and A.J. Collins. Comparative survival of dialysis patients in the united states after coronary angioplasty, coronary artery stenting, and coronary artery bypass surgery and impact of diabetes. *Circulation*, 106(17):2207, 2002.

[39] R.K. Myler, R.E. Shaw, S.H. Stertzer, H.S. Hecht, C. Ryan, J. Rosenblum, D.C. Cumberland, M.C. Murphy, H.N. Hansell, and B. Hidalgo. Lesion morphology and coronary angioplasty: current experience and analysis. *Journal of the American College of Cardiology*, 19(7):1641–1652, 1992.

[40] P.J. De Feyter, M. van den Brand, G.J. Laarman, R. Van Domburg, P.W. Serruys, and H. Suryapranata. Acute coronary artery occlusion during and after percutaneous transluminal coronary angioplasty. frequency, prediction, clinical course, management, and follow-up. *Circulation*, 83(3):927, 1991.

[41] M. Nobuyoshi, T. Kimura, H. Nosaka, S. Mioka, K. Ueno, H. Yokoi, N. Hamasaki, H. Horiuchi, and H. Ohishi. Restenosis after successful percutaneous transluminal coronary angioplasty: serial angiographic follow-up of 229 patients. *Journal of the American College of Cardiology*, 12(3):616, 1988.

[42] R. Heuser, F. Houser, S.D. Culler, E.R. Becker, S.L. Battaglia, L. Tarkington, and A.W. Simon. A retrospective study of 6,671 patients comparing coronary

stenting and balloon angioplasty. *Journal of Invasive Cardiology*, 12(7):354–354, 2000.

[43] S.E. Kimmel, A.R. Localio, C. Brensinger, C. Miles, J. Hirshfeld, H.L. Haber, and B.L. Strom. Effects of coronary stents on cardiovascular outcomes in broad-based clinical practice. *Archives of internal medicine*, 160(17):2593–2599, 2000.

[44] J.A. Bittl. Advances in coronary angioplasty. *New England Journal of Medicine*, 335(16):1290–1302, 1996.

[45] U. Sigwart, J. Puel, V. Mirkovitch, and L. Joffre, F. andKappen Berger. Intravascular stents to prevent occlusion and restenosis after transluminal angioplasty. *The New England Journal of Medicine*, 316(12):701–706, 1987.

[46] E.J. Topol and P.W. Serruys. Frontiers in interventional cardiology. *Circulation*, 98(17):1802, 1998.

[47] D.L. Fischman, M.B. Leon, D.S. Baim, R.A. Schatz, M.P. Savage, I. Penn, K. Detre, L. Veltri, D. Ricci, and M. Nobuyoshi. A randomized comparison of coronary-stent placement and balloon angioplasty in the treatment of coronary artery disease. stent restenosis study investigators. *The New England Journal of Medicine*, 331(8):496, 1994.

[48] S.G. Ellis, M.J. Cowley, P.L. Whitlow, M. Vandormael, A.M. Lincoff, G. DiSciascio, L.S. Dean, E.J. Topol, et al. Prospective case-control comparison of percutaneous transluminal coronary revascularization in patients with multivessel disease treated in 1986-1987 versus 1991: improved in-hospital and 12-month results. *Journal of the American College of Cardiology*, 25(5):1137–1142, 1995.

[49] D. Hasdai, K.N. Garratt, D.R. Holmes, et al. Coronary angioplasty and intracoronary thrombolysis are of limited efficacy in resolving early intracoronary

stent thrombosis. *Journal of the American College of Cardiology*, 28(2):361–367, 1996.

[50] K.H. Mak, G. Belli, S.G. Ellis, and D.J. Moliterno. Subacute stent thrombosis: evolving issues and current concepts. *Journal of the American College of Cardiology*, 27(2):494–503, 1996.

[51] D.R. Holmes. State of the art in coronary intervention. *The American journal of cardiology*, 91(3):50–53, 2003.

[52] A. Kastrati, A. Schomig, J. Dirschinger, J. Mehilli, N. von Welser, J. Pache, H. Schuhlen, T. Schilling, C. Schmitt, and F.J. Neumann. Increased risk of restenosis after placement of gold-coated stents: results of a randomized trial comparing gold-coated with uncoated steel stents in patients with coronary artery disease. *Circulation*, 101(21):2478, 2000.

[53] T.C. Woods and A.R. Marks. Drug-eluting stents. *Annu. Rev. Med.*, 55:169–178, 2004.

[54] P.W. Serruys, F. Unger, J.E. Sousa, A. Jatene, HJ Bonnier, JP Schonberger, N. Buller, R. Bonser, MJ Van Den Brand, LA Van Herwerden, et al. Comparison of coronary-artery bypass surgery and stenting for the treatment of multivessel disease. *N Engl J Med*, 344(15):1117–24, 2001.

[55] J.W. Moses, M.B. Leon, J.J. Popma, P.J. Fitzgerald, D.R. Holmes, C. OShaughnessy, R.P. Caputo, D.J. Kereiakes, D.O. Williams, P.S. Teirstein, et al. Sirolimus-eluting stents versus standard stents in patients with stenosis in a native coronary artery. *N Engl j Med*, 349(14):1315–23, 2003.

[56] E. Schampaert, E.A. Cohen, M. Schluter, F. Reeves, M. Traboulsi, et al. The canadian study of the sirolimus-eluting stent in the treatment of patients with

long de novo lesions in small native coronary arteries (c-sirius). *Journal of the American College of Cardiology*, 43(6):1110–1115, 2004.

[57] M.C. Morice, P.W. Serruys, J.E. Sousa, J. Fajadet, E. Ban Hayashi, M. Perin, A. Colombo, G. Schuler, P. Barragan, G. Guagliumi, et al. A randomized comparison of a sirolimus-eluting stent with a standard stent for coronary revascularization. *N Engl J Med*, 346(23):1773–80, 2002.

[58] K.R. Kamath, J.J. Barry, and K.M. Miller. The taxus (tm) drug-eluting stent: A new paradigm in controlled drug delivery. *Advanced drug delivery reviews*, 58(3):412–436, 2006.

[59] A. Colombo, J. Drzewiecki, A. Banning, E. Grube, K. Hauptmann, S. Silber, D. Dudek, S. Fort, F. Schiele, K. Zmudka, et al. Randomized study to assess the effectiveness of slow-and moderate-release polymer-based paclitaxel-eluting stents for coronary artery lesions. *Circulation*, 108(7):788, 2003.

[60] J. Daemen, E. Boersma, M. Flather, J. Booth, R. Stables, A. Rodriguez, G. Rodriguez-Granillo, W.A. Hueb, P.A. Lemos, and P.W. Serruys. Long-term safety and efficacy of percutaneous coronary intervention with stenting and coronary artery bypass surgery for multivessel coronary artery disease: a meta-analysis with 5-year patient-level data from the arts, eraci-ii, mass-ii, and sos trials. *Circulation*, 118(11):1146, 2008.

[61] K.B. Seung, D.W. Park, Y.H. Kim, S.W. Lee, C.W. Lee, M.K. Hong, S.W. Park, S.C. Yun, H.C. Gwon, M.H. Jeong, et al. Stents versus coronary-artery bypass grafting for left main coronary artery disease. *N Engl J Med*, 358(17):1781–92, 2008.

[62] W.E. Boden, R.A. Orourke, K.K. Teo, et al. Optimal medical therapy with or without pci for stable coronary disease (courage). *N Engl J Med*, 356(15):1503–16, 2007.

[63] C.P. Bailey, A. May, and W.M. Lemmon. Survival after coronary endarterectomy in man. *Journal of the american medical association*, 164(6):641, 1957.

[64] G.M. Fitzgibbon, H.P. Kafka, A.J. Leach, W.J. Keon, G.D. Hooper, and J.R. Burton. Coronary bypass graft fate and patient outcome: Angiographic follow-up of 5,065 grafts related to survival and reoperation in 1,388 patients during 25 years* 1. *Journal of the American College of Cardiology*, 28(3):616–626, 1996.

[65] A. Cameron, K.B. Davis, G. Green, and H.V. Schaff. Coronary bypass surgery with internal-thoracic-artery grafts-effects on survival over a 15-year period. *The New England journal of medicine*, 334(4):216–219, 1996.

[66] B.J. Leavitt, G.T. O'Connor, E.M. Olmstead, J.R. Morton, C.T. Maloney, L.J. Dacey, F. Hernandez, and S.J. Lahey. Use of the internal mammary artery graft and in-hospital mortality and other adverse outcomes associated with coronary artery bypass surgery. *Circulation*, 103(4):507, 2001.

[67] W.S. Weintraub, E.R. Becker, P.D. Mauldin, S. Culler, A.S. Kosinski, S.B. King, et al. Costs of revascularization over eight years in the randomized and eligible patients in the emory angioplasty versus surgery trial (east). *The American journal of cardiology*, 86(7):747–752, 2000.

[68] J.K. Kirklin. Prospects for understanding and eliminating the deleterious effects of cardiopulmonary bypass. *The Annals of thoracic surgery*, 51(4):529–531, 1991.

[69] R.M. Sniecinski and J.H. Levy. The inflammatory response to cardiopulmonary bypass. *On Bypass*, pages 125–140, 2008.

[70] E.R. Rosenkranz, F. Okamoto, G.D. Buckberg, J.M. Robertson, J. Vinten-Johansen, and H.I. Bugyi. Safety of prolonged aortic clamping with blood cardioplegia. iii. aspartate enrichment of glutamate-blood cardioplegia in energy-

depleted hearts after ischemic and reperfusion injury. *The Journal of Thoracic and Cardiovascular Surgery*, 91(3):428, 1986.

[71] T.C. Koutlas, J.R. Elbeery, J.M. Williams, J.F. Moran, N.A. Francalancia, and W.R. ChitwoodJr. Myocardial revascularization in the elderly using beating heart coronary artery bypass surgery. *The Annals of thoracic surgery*, 69(4):1042–1047, 2000.

[72] M.J. Mack, T.M. Dewey, and M.J. Magee. Facilitated anastomosis for reoperative circumflex coronary revascularization on the beating heart through a left thoracotomy. *The Journal of Thoracic and Cardiovascular Surgery*, 123(4):816, 2002.

[73] M. Guler, K. Kirali, M.E. Toker, N. Bozbua, S.N. Omerolu, E. Akinci, and C. Yakut. Different cabg methods in patients with chronic obstructive pulmonary disease. *The Annals of thoracic surgery*, 71(1):152–157, 2001.

[74] R. Ascione, S. Williams, C.T. Lloyd, T. Sundaramoorthi, A.A. Pitsis, and G.D. Angelini. Reduced postoperative blood loss and transfusion requirement after beating-heart coronary operations: a prospective randomized study. *The Journal of thoracic and cardiovascular surgery*, 121(4):689, 2001.

[75] R. Ascione, C.T. Lloyd, W.J. Gomes, M. Caputo, A.J. Bryan, and G.D. Angelini. Beating versus arrested heart revascularization: evaluation of myocardial function in a prospective randomized study1. *European journal of cardiothoracic surgery*, 15(5):685–690, 1999.

[76] M.E. Plomondon, J.C. Cleveland Jr, S.T. Ludwig, G.K. Grunwald, C.I. Kiefe, F.L. Grover, and A.L. Shroyer. Off-pump coronary artery bypass is associated with improved risk-adjusted outcomes. *The Annals of thoracic surgery*, 72(1):114, 2001.

[77] V.I. Kolessov. Mammary artery-coronary artery anastomosis as method of treatment for angina pectoris. *The Journal of thoracic and cardiovascular surgery*, 54(4):535, 1967.

[78] A. Lichtenberg, C. Hagl, W. Harringer, U. Klima, and A. Haverich. Effects of minimal invasive coronary artery bypass on pulmonary function and postoperative pain. *The Annals of thoracic surgery*, 70(2):461, 2000.

[79] J. Bonatti, R. Ladurner, H. Antretter, C. Hormann, G. Friedrich, N. Moes, V. Muhlberger, and O. Dapunt. Single coronary artery bypass grafting-a comparison between minimally invasive "off pump" techniques and conventional procedures. *European journal of cardio-thoracic surgery*, 14:7–12, 1998.

[80] R.C. King, T.B. Reece, J.L. Hurst, K.S. Shockey, C.G. Tribble, W.D. Spotnitz, and I.L. Kron. Minimally invasive coronary artery bypass grafting decreases hospital stay and cost. *Annals of surgery*, 225(6):805, 1997.

[81] J. Bonatti, T. Schachner, N. Bonaros, A. Ohlinger, M. Danzmayr, P. Jonetzko, G. Friedrich, C. Kolbitsch, P. Mair, and G. Laufer. Technical challenges in totally endoscopic robotic coronary artery bypass grafting. *The Journal of Thoracic and Cardiovascular Surgery*, 131(1):146, 2006.

[82] J. Bonatti, T. Schachner, N. Bonaros, A. Oehlinger, D. Wiedemann, E. Ruetzler, F. Weidinger, C. Kolbitsch, G. Feuchtner, D. Zimrin, et al. Effectiveness and Safety of Total Endoscopic Left Internal Mammary Artery Bypass Graft to the Left Anterior Descending Artery. *The American journal of cardiology*, 104(12):1684–1688, 2009.

[83] S. Dogan, T. Aybek, et al. Totally endoscopic coronary artery bypass grafting on cardiopulmonary bypass with robotically enhanced telemanipulation: report of forty-five cases. *The Journal of Thoracic and Cardiovascular Surgery*, 123(6):1125, 2002.

[84] S. Srivastava, S. Gadasalli, M. Agusala, R. Kolluru, J. Naidu, M. Shroff, R. Barrera, S. Quismundo, and V. Srivastava. Use of bilateral internal thoracic arteries in CABG through lateral thoracotomy with robotic assistance in 150 patients. *The Annals of thoracic surgery*, 81(3):800, 2006.

[85] V.A. Subramanian, N.U. Patel, N.C. Patel, and D.F. Loulmet. Robotic assisted multivessel minimally invasive direct coronary artery bypass with port-access stabilization and cardiac positioning: paving the way for outpatient coronary surgery? *The Annals of thoracic surgery*, 79(5):1590–1596, 2005.

[86] B. Kiaii, R.S. McClure, L. Stitt, R. Rayman, W.B. Dobkowski, G. Jablonsky, R.J. Novick, and W.D. Boyd. Prospective angiographic comparison of direct, endoscopic, and telesurgical approaches to harvesting the internal thoracic artery. *The Annals of thoracic surgery*, 82(2):624–628, 2006.

[87] F. Robicsek. Robotic cardiac surgery: Time told! *The Journal of Thoracic and Cardiovascular Surgery*, 135(2):243, 2008.

[88] S. Srivastava, S. Gadasalli, M. Agusala, R. Kolluru, R. Barrera, S. Quismundo, U. Kreaden, and V. Jeevanandam. Beating heart totally endoscopic coronary artery bypass. *The Annals of thoracic surgery*, 89(6):1873, 2010.

[89] C. Gao, M. Yang, Y. Wu, G. Wang, C. Xiao, Y. Zhao, and J. Wang. Early and midterm results of totally endoscopic coronary artery bypass grafting on the beating heart. *The Journal of Thoracic and Cardiovascular Surgery*, 2011.

[90] M. Argenziano, M. Katz, J. Bonatti, S. Srivastava, D. Murphy, R. Poirier, D. Loulmet, L. Siwek, U. Kreaden, and D. Ligon. Results of the prospective multicenter trial of robotically assisted totally endoscopic coronary artery bypass grafting. *The Annals of thoracic surgery*, 81(5):1666–1675, 2006.

[91] V. Falk, A. Diegeler, T. Walther, S. Jacobs, J. Raumans, and FW Mohr. Total endoscopic off-pump coronary artery bypass grafting. *Heart Surgery Forum*, 3(1):29–31, 2000.

[92] P. Modi, E. Rodriguez, and W.R. Chitwood Jr. Robot-assisted cardiac surgery. *Interactive CardioVascular and Thoracic Surgery*, 9(3):500, 2009.

[93] R.J. Damiano Jr. Robotics in cardiac surgery: The emperor's new clothes. *The Journal of Thoracic and Cardiovascular Surgery*, 134(3):559, 2007.

[94] D. de Canniere, G. Wimmer-Greinecker, R. Cichon, V. Gulielmos, F. Van Praet, U. Seshadri-Kreaden, and V. Falk. Feasibility, safety, and efficacy of totally endoscopic coronary artery bypass grafting: Multicenter European experience. *The Journal of Thoracic and Cardiovascular Surgery*, 134(3):710–716, 2007.

[95] M. Figl, D. Rueckert, D. Hawkes, R. Casula, M. Hu, O. Pedro, D.P. Zhang, G. Penney, F. Bello, and P. Edwards. Image guidance for robotic minimally invasive coronary artery bypass. *Computerized Medical Imaging and Graphics*, 34(1):61–68, 2010.

[96] A.L. Trejos, R.V. Patel, I. Ross, and B. Kiaii. Optimizing port placement for robot-assisted minimally invasive cardiac surgery. *The International Journal of Medical Robotics and Computer Assisted Surgery*, 3(4):355–364, 2007.

[97] V. Falk, F. Mourgues, L. Adhami, S. Jacobs, H. Thiele, S. Nitzsche, F.W. Mohr, and E. Coste-Maniere. Cardio navigation: planning, simulation, and augmented reality in robotic assisted endoscopic bypass grafting. *The Annals of thoracic surgery*, 79(6):2040–2047, 2005.

[98] C. Hartung, C. Gnahm, R. Friedl, M. Hoffmann, and K. Dietmayer. Computer-assisted LAD bypass grafting at the open heart. In *Proceedings of SPIE*, volume 7261, page 72610P, 2009.

[99] X. Huang, J. Moore, G. Guiraudon, D.L. Jones, D. Bainbridge, J. Ren, and T.M. Peters. Dynamic 2d ultrasound and 3d ct image registration of the beating heart. *Medical Imaging, IEEE Transactions on*, 28(8):1179–1189, 2009.

[100] D.G. Gobbi, R.M. Comeau, and T.M. Peters. Ultrasound probe tracking for real-time ultrasound/MRI overlay and visualization of brain shift. In C. Taylor and A. Colchester, editors, *Medical Image Computing and Computer-Assisted Interventions - MICCAI 1999*, volume LNCS 1679, pages 920–927. Springer, Cambridge, UK, 1999.

[101] C.A. Linte, M. Wierzbicki, J. Moore, S.H. Little, G.M. Guiraudon, and T.M. Peters. Towards subject-specific models of the dynamic heart for image-guided mitral valve surgery. In *Proceedings of the 10th international conference on Medical image computing and computer-assisted intervention*, pages 94–101. Springer-Verlag, 2007.

[102] P. Lang, E.C.S. Chen, G.M. Guiraudon, D.L. Jones, D. Bainbridge, M.W. Chu, M. Drangova, N. Hata, A. Jain, and T.M. Peters. Feature-based us to ct registration of the aortic root. In *Proceedings of SPIE*, volume 7964, page 79641G, 2011.

[103] K. Darabi, P. Grunert, and A. Perneczky. Accuracy of intraoperative navigation using skin markers. In *Computer Assisted Radiology and Surgery*, pages 920–924, 1997.

[104] R.S. Lazebnik, T.L. Lancaster, M.S. Breen, J.S. Lewin, and D.L. Wilson. Volume registration using needle paths and point landmarks for evaluation of interventional MRI treatments. *Medical Imaging, IEEE Transactions on*, 22(5):653–660, 2003.

[105] C.R. Maurer Jr, J.M. Fitzpatrick, M.Y. Wang, R.L. Galloway Jr, R.J. Maciunas,

and G.S. Allen. Registration of head volume images using implantable fiducial markers. *Medical Imaging, IEEE Transactions on*, 16(4):447–462, 1997.

[106] P.A. Woerdeman, P.W.A. Willems, H.J. Noordmans, C.A.F. Tulleken, and J.W.B. van der Sprenkel. Application accuracy in frameless image-guided neurosurgery: a comparison study of three patient-to-image registration methods. *Journal of neurosurgery*, 106(6):1012–1016, 2007.

[107] D. Jones, D.A. Christopherson, J.T. Washington, M.D. Hafermann, J.W. Rieke, J.J. Travaglini, and S.S. Vermeulen. A frameless method for stereotactic radiotherapy. *British journal of radiology*, 66(792):1142, 1993.

[108] S.B. Park, F.C. Rhee, J.I. Monroe, and J.W. Sohn. Spatially weighted mutual information image registration for image guided radiation therapy. *Medical physics*, 37:4590, 2010.

[109] C.A. Linte, M. Carias, D.S. Cho, D.F. Pace, J. Moore, C. Wedlake, D. Bainbridge, B. Kiaii, and T.M. Peters. Estimating heart shift and morphological changes during minimally invasive cardiac interventions. In *Proceedings of SPIE*, volume 7625, page 762509, 2010.

[110] J.G. Parker, B.A. Mair, and D.R. Gilland. Respiratory motion correction in gated cardiac SPECT using quaternion-based, rigid-body registration. *Medical physics*, 36:4742, 2009.

[111] J. Sra, D. Krum, A. Malloy, M. Vass, B. Belanger, E. Soubelet, R. Vaillant, and M. Akhtar. Registration of three-dimensional left atrial computed tomographic images with projection images obtained using fluoroscopy. *Circulation*, 112(24):3763, 2005.

[112] B.K.P. Horn et al. Closed-form solution of absolute orientation using unit quaternions. *Journal of the Optical Society of America A*, 4(4):629–642, 1987.

[113] K.S. Arun, T.S. Huang, and S.D. Blostein. Least-squares fitting of two 3-D point sets. *Pattern Analysis and Machine Intelligence, IEEE Transactions on*, (5):698–700, 1987.

[114] P.J. Besl and N.D. McKay. A method for registration of 3-D shapes. *IEEE Transactions on pattern analysis and machine intelligence*, pages 239–256, 1992.

[115] B. Ma. Robust surface-based registration from sparse measurements. MSc thesis, Queen's University at Kingston, 1999.

[116] JB Maintz and M.A. Viergever. A survey of medical image registration. *Medical image analysis*, 2(1):1–36, 1998.

[117] J.M. Fitzpatrick, J.B. West, and C.R. Maurer Jr. Predicting error in rigid-body point-based registration. *Medical Imaging, IEEE Transactions on*, 17(5):694–702, 1998.

[118] J.M. Fitzpatrick. Fiducial registration error and target registration error are uncorrelated. In *Proc. of SPIE Vol*, volume 7261, pages 726102–1, 2009.

[119] J.T. Moore, A.D. Wiles, C. Wedlake, D. Bainbridge, B. Kiaii, A.L. Trejos, R. Patel, and T.M. Peters. Integration of trans-esophageal echocardiography with magnetic tracking technology for cardiac interventions. In *Proceedings of SPIE*, volume 7625, page 76252Y, 2010.

[120] A.D. Wiles, D.G. Thompson, and D.D. Frantz. Accuracy assessment and interpretation for optical tracking systems. In *Proc. SPIE*, volume 5367, pages 421–32, 2004.

[121] W. Press, B. Flannery, S.A. Teukolsky, and W.T. Vetterling. *Numerical recipes in C*, chapter 10.4, pages 408–412. Cambridge university press Cambridge, 2007.

[122] M.J. Black, G. Sapiro, D.H. Marimont, and D. Heeger. Robust anisotropic diffusion. *IEEE Transactions on Image Processing*, 7(3):421–432, 1998.

[123] P. Yushkevich, J Piven, C Hazlett, H Smith, G Smith, R Ho, S Ho, J Gee, and G Gerig. User-guided 3d active contour segmentation of active contour segmentation of anatomical structures: Significantly improved efficiency and reliability. *Neuroimage*, 31(3):1116–1128, 2006.

[124] P. Aljabar, R.A. Heckemann, A. Hammers, J.V. Hajnal, and D. Rueckert. Multi-atlas based segmentation of brain images: Atlas selection and its effect on accuracy. *Neuroimage*, 46(3):726–738, 2009.